HIGH MAGNIFICATION
POLYMERIC LENS FOR SMARTPHONE MICROSCOPE

Miss Wisansaya Jaikeandee

A Thesis Submitted in Partial Fulfillment of the Requirements
for the Degree of Master of Science in Petrochemistry and Polymer
Science
Field of Study of Petrochemistry and Polymer Science
Faculty of Science
Chulalongkorn University
Academic Year 2019
Copyright of Chulalongkorn University

เลนส์พอลิเมอร์กำลังขยายสูงสำหรับกล้องจุลทรรศน์สมาร์ตโฟน

น.ส.วิศัลย์ศยา ใจเขียนดี

วิทยานิพนธ์นี้เป็นส่วนหนึ่งของการศึกษาตามหลักสูตรปริญญาวิทยาศาสตรมหาบัณฑิต
สาขาวิชาปิโตรเคมีและวิทยาศาสตร์พอลิเมอร์ สาขาวิชาปิโตรเคมีและวิทยาศาสตร์พอลิเมอร์
คณะวิทยาศาสตร์ จุฬาลงกรณ์มหาวิทยาลัย
ปีการศึกษา 2562

Thesis Title	HIGH MAGNIFICATION POLYMERIC LENS FOR SMARTPHONE MICROSCOPE
By	Miss Wisansaya Jaikeandee
Field of Study	Petrochemistry and Polymer Science
Thesis Advisor	Professor SANONG EKGASIT, Ph.D.
Thesis Co Advisor	Jariya Buacharern, Ph.D.

Accepted by the Faculty of Science, Chulalongkorn University in Partial Fulfillment of the Requirement for the Master of Science

-- Dean of the Faculty of Science
()

THESIS COMMITTEE

-- Chairman
(Assistant Professor WARINTHORN CHAVASIRI, Ph.D.)

-- Thesis Advisor
(Professor SANONG EKGASIT, Ph.D.)

-- Thesis Co-Advisor
(Jariya Buacharern, Ph.D.)

-- Examiner
(Prasit Pattananuwat, Ph.D.)

-- External Examiner
(Assistant Professor Toemsak Srikhirin, Ph.D.)

จุฬาลงกรณ์มหาวิทยาลัย

CHULALONGKORN UNIVERSITY

วิศัลย์ศยา ใจเขียนดี : เลนส์พอลิเมอร์กำลังขยายสูงสำหรับกล้องจุลทรรศน์สมาร์ตโฟน. (
HIGH MAGNIFICATION
POLYMERIC LENS FOR SMARTPHONE MICROSCOPE) อ.ที่ปรึกษาหลัก :
ศ. ดร.สนอง เอกสิทธิ์, อ.ที่ปรึกษาร่วม : ดร.จริยา บัวเจริญ

ในงานวิจัยนี้จึงนำเสนอการขึ้นรูปเลนส์พอลิเมอร์ชนิดเลนส์นูนแกมระนาบด้วยพอลิเมอร์ที่มีค่าดัชนีหักเหสูง

แตกต่างกัน 2 ชนิด คือ พอลิไดเมทิลไซลอกเซน (พีดีเอ็มเอส, $n \sim 1.42$) และนอร์แลนด์ออพติคัลแอดฮีพซีฟ 61 (เอ็นโอ

เอ 61, $n \sim 1.56$) โดยอาศัยเทคนิคการหยดแบบตรึงที่จำกัดขอบเขต ซึ่งเป็นเทคนิคที่มีขั้นตอนในการขึ้นรูปเลนส์อย่างง่าย

และสามารถควบคุมรูปร่างของเลนส์ได้ผ่านการหยดพอลิเมอร์เหลวที่มีการควบคุมน้ำหนักลงบนฐานรองรับที่ทำจากแผ่นวงกลม

อะคริลิค และฐานรองรับมีการขึ้นรูปผ่านพีดีเอ็มเอสบาง ๆ ที่ถูกนำมาเจาะแผ่นวงกลมมีเส้นผ่าศูนย์กลางตั้งแต่ 2.5-6.0

มิลลิเมตร พอลิเมอร์เหลวจะแพร่กระจายอย่างสมมาตรทุกทิศทางบนฐานรองรับ และถูกตึงด้วยขอบคมของฐานรองรับภายใต้

ความสมดุลระหว่างแรงโน้มถ่วงและแรงตึงผิวระหว่างผิวหน้า ทำให้พอลิเมอร์ก่อตัวได้เป็นเลนส์ที่มีความโค้งนูนและมีผิวหน้า

เลนส์ที่เรียบ นอกจากนี้พบว่าเมื่อมีการใช้น้ำหนักของพอลิเมอร์เหลวบนถูกหยดบนฐานรองรับเพิ่มมากขึ้น ทำให้รูปร่างของ

เลนส์เบี่ยงเบน เนื่องจากได้รับอิทธิพลจากแรงโน้มถ่วงจ เลนส์พอลิเมอร์ที่ผลิตได้มีกำลังขยายสูงสุดอยู่ที่ 51.0 เท่า และ

88.3 เท่า สำหรับเลนส์พอลิไดเมทิลไซลอกเซน และเลนส์นอร์แลนด์ออพติคัลแอดฮีพซีฟ 61 ตามลำดับ นอกจากนี้คุณภาพ

การถ่ายภาพของเลนส์พอลิเมอร์ถูกกำหนดโดยใช้ USAF 1951 target ทำให้เลนส์พอ-ลิเมอร์สามารถใช้เปลี่ยนสมาร์ต

โฟนให้เป็นกล้องจุลทรรศน์สมาร์ตโฟนให้สามารถบันทึกภาพสิ่งเล็กๆ ที่ไม่สามารถมองเห็นด้วยตาเปล่าได้ อย่างไรก็ตามด้วย

ค่าดัชนีหักเหที่สูงของเลนส์นูนที่ถูกขึ้นรูปด้วยนอร์แลนด์ออพติคัลแอดฮีพซีฟ 61 ทำให้สามารถนำมาใช้ในการออกแบบ

สาขาวิชา	ปิโตรเคมีและวิทยาศาสตร์พอลิเมอร์	ลายมือชื่อนิสิต..
ปีการศึกษา	2562	ลายมือชื่อ อ.ที่ปรึกษาหลัก..............................
		ลายมือชื่อ อ.ที่ปรึกษาร่วม................................

5972059123 : MAJOR PETROCHEMISTRY AND POLYMER SCIENCE
KEYWOR   NOA 61, SPR sensor chip, Sylgard 184, polymeric lens
D:

Wisansaya   Jaikeandee   :   HIGH MAGNIFICATION
POLYMERIC LENS FOR SMARTPHONE MICROSCOPE.   Advisor:
Prof. SANONG EKGASIT, Ph.D. Co-advisor: Jariya Buacharern, Ph.D.

In this work, we present a facile method for fabrication of plano-convex
lenses, using high reflective optical polymer (Polydimethylsiloxane, Sylgard 184 by
Dow Corning, n ~1.42 and Norland Optical adhesive 61, NOA61 by Norland
Products, ~1.56) under the confined sessile drop technique. The confined sessile
drop technique is a facile method and an adjustable lens geometry through
controlled the weight of liquid polymer on the lens substrate, as PMMA circular
disk and Sylgard circular disk, with different diameter (2.5-6.0 mm). The liquid
polymer was gradually spread and radially over the surface of the lens substrate,
and resistance to spreading of liquid by a sharp edge under the gravitational force
and interfacial surface tension to form spherical cap with smooth surface. When the
use of the weight of liquid polymer increased, the deformation of the lens observed
due to affect the gravitational force. The fabricated lenses, as Sylgard 184 plano-
convex lens and NOA 61 plano-convex lens, provides the magnification up to
51.0X and 88.3X, respectively. In addition, the imaging quality of the fabricated
lenses was characterized using USAF 1951 target. The fabricated plano-convex

Field of Study:	Petrochemistry and Polymer Science	Student's Signature ....
Academic Year:	2019	Advisor's Signature ....
		Co-advisor's Signature ....

ACKNOWLEDGEMENTS

TABLE OF CONTENTS

LIST OF TABLES

LIST OF FIGURES

LIST OF ABBREVIATIONS AND SYMBOLS

Sylgard 184	:	Polydimethylsiloxane
NOA 61	:	Norland Optical Adhesive 61
PMMA	:	Polymethylmethacrylate
The fabricated lenses	:	Sylgard 184 plano-convex lens and
		NOA 61 plano-convex lens
NOA 65	:	Norland Optical Adhesive 65
NOA 73	:	Norland Optical Adhesive 73
NOA 81	:	Norland Optical Adhesive 81
NOA 88	:	Norland Optical Adhesive 88
NOA 13685	:	Norland Optical Adhesive 13685
NOA 1625	:	Norland Optical Adhesive 1625
NEA 121	:	Norland Electronic Adhesive 121
ZnO	:	Zinc oxide
NPs	:	Nanoparticles
ODT	:	1,8-Octanedithiol
GLC	:	Gas-liquid chromatography
LOC	:	Lap-on-a-chip
AgNPs	:	Silver nanoparticles
H_2O_2	:	Hydrogen peroxide
PCB	:	Printed Circuit Boards
MLAs	:	Microlens Arrays

SPR	:	Surface Plasmon Resonance
θ_e	:	Equilibrium contact angle
θ_c	:	Critical contact angle
θ	:	Contact angle
ϕ	:	The subtended angle at the edge
$\emptyset$	:	Diameter of the lens substrate (mm)
f	:	Focal length (mm)
D	:	Diameter of lens (mm)
r	:	Radius of lens (mm)
R	:	Radius of lens curvature (mm)
H	:	Height of lens (mm)
n	:	Refractive index
°C	:	Degree Celsius
% wt, % w/w	:	Weight by weight percent
μm	:	Micrometer
mm	:	Millimeter
cm	:	Centimeter
nm	:	Nanometer
cm^{-1}	:	Reciprocal centimeter
h	:	Hour
min	:	minute
kg/m^3	:	Kilogram per liter
cps	:	Centipoise

Dyne/cm : Dyne per centimeter

Volts/mil : Volts per mil (a mil is 1/1000 inch)

$\Omega \cdot cm$: Ohm centimeter

CHAPTER I

INTRODUCTION

Lenses are important optical components of microscopes and telescopes employed for focusing or diverging light beam into an optical system. The lenses are usually made from glass or transparent material with an appropriate index of refraction, such as crystals, transparent polymers, and UV-curable polymers, etc. For the high-quality glass lens, multi-step manufacturing, including injection molding, shaping, and mechanical polishing, is essential to produce an optically smooth surface with appropriate size. This result in the costly production of the high-quality glass lens. Whereas, the polymeric lens is another class of lenses made from optical polymers. The polymeric lens possesses characteristic advantages, including easy fabrication, controllable refractive index, high mechanical strength, and chemical and thermal resistant, etc. The usage of the polymeric lens has increased and has designed to be used in some applications instead of a common glass lens. The polymeric lens can be fabricated by many techniques, such as replica molding, thermal reflow, hanging drop, free surface sharping modifies the surface, drop on demand, inkjet printing, confined inkjet printing, and confined sessile drop technique. The various fabricated techniques produced various types of polymeric lenses. Those polymeric lenses have utilized in the unique applications, such as optical component

fabrication[1-8], light-emitting device [9-12], fiber coupler [13, 14], monolithic diamond Raman laser [15]. The types of polymeric lens, including ball, biconvex, concave, aspheric, and plano-convex lens, were classified by the lens surfaces with at reach one curved surface. The plano-convex lens has one convex surface and one flat surface. It was mostly fabricated by transparent polymers, such as an elastomeric polymer or UV-curable polymers. The popular elastomeric polymer is known as polydimethylsiloxane (PDMS, Sylgard 184). Sylgard 184 is the elastomeric polymer with a refractive index of 1.42. It has been used for generation of elastomeric molds for micro-lenses replication. Nevertheless, it has also utilized to create the pattern of micro-lenses and micro-lens arrays which later employed for the fabrication of UV-curable polymer micro-lenses.

Recently, advance smartphone technology has been extensively developed. The high-performance smartphone has rapidly released to the global market at an affordable price. The distinctive advantages of smartphone, for example, powerful processing, high-performance image sensors, ease of connectivity (4G, Wi-Fi, Bluetooth), high mobility and power supply free, enable the development of scientific smartphone accessories that can turn the common smartphone to the point-of-care devices. Those point-of-care devices have been utilized anywhere outside the laboratory at the point of need. Together with a smartphone camera, the Sylgard 184 plano-convex lens has been attached to the camera lens converting the common smartphone to smartphone microscope. The smartphone microscope provides exceptional performance for microscopy similar to the common optical microscope. It has been used for taking the image of micro-size objects, such as, vein and stomata of leaf [8], human skin and hair follicle cross-section histology slide [16], slice of human

colon [5], Printed Circuit Boards (PCB) [6, 8], default on gunshot residue [17], and bullet tool marks [17].

Although the Sylgard 184 is the promising material for making optics that achieve long-term performance under rough environment conditions, however, it can easily collect dust and it shows minimal aging (yellowing). Low rigidity and refractive index limit the production of high-quality optics from Sylgard 184. Due to the limitation of Sylgard 184, the UV-curable polymers had become an interesting material for the fabrication of polymeric lens. One of the interesting UV-curable polymers is Norland Optical Adhesive 61 (NOA 61). NOA 61 is the adhesive UV-curable polymer that has distinctive properties, including, excellent clarity, high optically transparent (>95%) in the UV-NIR region, low shrinkage, highly chemical resistant, and inert. The NOA 61 has the rigidity and the high refractive index suitably for making high-quality optics. Although there is a report that demonstrates the fabrication of NOA 61 lens using a Si-wafer frame and Sylgard 184 molding, they still found a fluctuation in image quality due to its small size and lustrous surface.

In this work, we demonstrate a simple yet efficient technique for fabrication of Sylgard 184 and NOA 61 plano-convex lenses using the confined sessile drop technique. The lens geometry could be precisely controlled by adjusting the amount of liquid polymer. The effect of lens geometry on lens parameters including, focal length, contact angle, lens diameter, were systematically investigated. The fabricated plano-convex lenses were utilized as the smartphone accessory that could turn the smartphone to smartphone microscope. The Sylgard 184 and NOA 61 plano-convex lens were attached on a smartphone camera. The quality of digital micrographs taken from the fabricated lenses was evaluated. Since the NOA 61 plano-convex lens has

high index of reflection, we further investigate the utilization of NOA 61 plano-convex lens as a miniature SPR prism. The Kretschmann SPR configuration was obtained by forming a thin Cr/Au film on the planar side of NOA 61 plano-convex lens. The performance of miniature SPR prism was evaluated

1.1 The objectives

1. To fabricate the plano-convex lenses from polydimethylsiloxane (PDMS, Sylgard 184) and Norland optical adhesive 61 (NOA 61) using confined sessile drop technique.

2. To demonstrate the potential of polymeric plano-convex lenses as an external lens for a smartphone that can turn the smartphone to the smartphone microscope.

3. To demonstrate the potential polymeric plano-convex lenses as an effective miniature SPR prism for disposable and economical SPR sensor chip.

1.2 Scopes of research

1. Development of the confined sessile drop technique for fabrication of the plano-convex lens from Sylgard 184 and NOA 61

2. Study the properties of polymer that affect lens formation, i.e. refractive index, viscosity, and shrinkage of polymer.

3. Study the relationship between the weight of the liquid polymer and the contact angle (θ) of liquid polymer at the edge of lens substrate, which affects the geometries of the fabricated plano-convex lens.

4. Study the relationship between the contact angle (θ) of liquid polymer and the optical parameters of the fabricated plano-convex lens, i.e. focal length (f) and magnification (M).

5. Evaluation of the resolution and the contrast of the fabricated lenses using a 1951 USAF resolution target.

6. Study the applications of the fabricated lenses as an external-optical microscope lens on the mobile phone camera and the miniature SPR sensor chip.

จุฬาลงกรณ์มหาวิทยาลัย
CHULALONGKORN UNIVERSITY

CHARTER II

THEORETICAL BACKGROUND

2.1 Polymeric lens fabrication techniques

2.1.1   Fabrication techniques

The polymeric lenses are usually produced as small lenses with a diameter often less than or as same as a millimeter (mm). Due to the small size of lenses, it was easy to develop the fabrication technique which forms in a single production step. The small lens which has a diameter as less than 10 micrometers (μm), calls microlens. Mostly, the microlens can form a microlens array (MLAs) or a single microlens, which depends on its applications. For instance, the microlens arrays (MLAs) were fabricated for use as a light diffuser [9], integral and enhanced light collections [18], and anti-reflection coatings [19]. In the cases of single microlenses, such as biconvex lens, aspherical lens, and plano-convex lens, were fabricated for use as visualization in optocapillary flow manipulation [20], and external lens for smartphone microscopes [5, 6, 8, 16, 17, 21, 22]. Due to the variety of applications, various fabrication techniques were developed. The fabrication techniques need to be simple and have ability enough to precisely control the lens properties which are height of lens, lens diameter, radius of lens curvature, contact angle, and focal length. In addition, high reproducibility and productivity were also essential.

In the past two decades, the polymeric lenses were fabricated in several techniques, including, replica molding [9, 22-26], thermal reflow [15, 18, 27-30], self-assembly technique [10, 13, 20, 31], hanging drop [5-8], free surface sharping [4], modifies surface [32], drop on demand [1, 33], inkjet printing [16, 19, 33], confined inkjet printing [34], and confined sessile drop technique [17, 35]. Each of these techniques possesses lens fabrication using different polymer, or different controllable of lens parameters which are the height of the lens, lens diameter, radius of lens curvature, contact angle, and focal length. The comparisons of fabrication techniques, including, lens materials, types of lens, and the distinctive technique, are shown in Table 2.1.

Although several lens fabrication techniques were developed, some techniques remained to use an expensive and complex machine. Thus, the development of a simple and reliable method for the fabrication of polymeric lens is still essential.

จุฬาลงกรณ์มหาวิทยาลัย
CHULALONGKORN UNIVERSITY

Table 2.1 Lists of fabrication techniques

Fabrication techniques	Material (Refractive index, n)	Type of lens	Distinctive points	Ref.
Replica molding	Sylgard 184 (1.41)	MLAs	- Controlled height of micro lens by diameters of holes micro-drilled - Used Sylgard 184 MLAs as light diffuser	[9]
Replica molding	NOA81 (1.56), and NOA 13685 (1.3685)	MLAs	- Controlled lens diameter by the parameters of laser printed microdroplets that corresponding to design size and shape of Sylgard 184 mold - Controlled magnification by refractive index of polymer.	[24]
Drop on demand (DOD)	UV-curable polymer (1.532)	Concave micro-lenses	- Reported simple and cost-effective fabrication method for micro-lenses. - Used UV-curable polymer for fabricated lens - Controlled radius of lens curvature by adjusted the speed curing time of UV polymer	[33]

Table 2.1 Lists of fabrication techniques (Continues)

Fabrication techniques	Material (Refractive index, n)	Type of lens	Distinctive points	Ref.
Drop on demand (DOD)	NOA 1625 (1.625)	MLAs	- Controlled contact angle by varies volume of polymer - Reported the achievement of spherical-like microlens formation with a perfect curvature	[1]
Thermal reflow process	Sylgard 184 (1.42)	MLAs	- Controlled lens diameter through changing reflow temperature in range of 115-140°C - Used MLAs for integration and enhancement light collections of the fluorescent signal	[18]
Thermal reflow process	Diamond (2.42)	Diamond MLAs	- Designed a large diamond MLAs - Controlled radius of curvature by design diameter size of mold and height holder from NOA 81 - Used as monolithic diamond Raman lasers with a high conversion efficiency.	[15]

Table 2.1 Lists of fabrication techniques (Continues)

Fabrication techniques	Material (Refractive index, n)	Type of lens	Distinctive points	Ref.
Thermal reflow process	UV-resin, GA-126 (1.4887)	MLAs	- Controlled focal length through the refractive index of polymer - Can reuse the master mold for fabricated lens - Used MLAs for detects each small part of wavefront and focuses on the image sensor for Shack–Hartmann wavefront sensors (SHWSs)	[28]
Replica molding	Glass	Glass MLAs	- Designed low cost fabrication method for a high-surface-quality glass MLAs. - Controlled size of lens by design VC mold and glass mold fabrication	[25]
Replica molding	Sylgard 184 (1.406)	Spherical microlens	- Controlled focal length and lens diameter by deposited/curing temperature of Sylgard 184 in the range 65-130°C. - Obtained focal length ranged from 2 to 25 mm, lens diameter 450 to 4 mm, and height of lens 14-600 mm	[26]

Table 2.1 Lists of fabrication techniques (Continues)

Fabrication techniques	Material (Refractive index, n)	Type of lens	Distinctive points	Ref.
Self-assembled	A mixture of 85 %wt NOA65 and 15 %wt acetone (1.524)	Plano-convex MLAs and biconvex MLAs	- Demonstrate the plano-convex lens and biconvex lenses fabrication method - Controlled aperture and surface profile by the photomask and volume of polymer, respectively.	[10]
Self-assembled	Sylgard 184 (1.42)	Plano-convex lens	- Controlled shape and size of the microlenses through curing time that allowed the temperature. - Used the Sylgard 184 micro lens in optocapillary flow manipulation	[20]
Self-assembled	NOA 73 (1.56)	MLAs	- Controlled focal length by the volume of droplet inside each circular hole - Have a potential coupling light in three-dimensional system	[31]

Table 2.1 Lists of fabrication techniques (Continues)

Fabrication techniques	Material (Refractive index, n)	Type of lens	Distinctive points	Ref.
Hanging drop	Sylgard 184 (1.42)	Parabolic lens	- Reported a low-cost fabrication methods for designed a high performance lenses - Used the fabricated lens for reduced the light diverging from the LED element. - Used as a smartphone microscope	[5]
Hanging drop	Sylgard 184 (1.42)	Aspheric lens	- Controlled shape and focal length by volume of liquid polymer and reversibly substrate - Studied an effect of inverted gravitational force. - Used the fabricated lenses as a commercially available smartphone camera	[8]
Hanging drop	Sylgard 184 (1.42)	Aspheric MLAs	- Controlled focal length by volume of liquid polymer on heat-assisted forces with substrate. - Used as a smartphone microscope	[6]

Table 2.1 Lists of fabrication techniques (Continues)

Fabrication techniques	Material (Refractive index, n)	Type of lens	Distinctive points	Ref.
Free surface shaping	NEA 121 (300 cps), NOA 61 (1.56, 300 cps) NOA 88 (1.56)	Plano-convex lens	- Fabricated adhesive lenses by 3 UV-curable polymers as NEA 121, NOA 61, NOA 88 that have difference viscosity and refractive index - Controlled lens diameter of the fabricated lens through size of SU-8th master and Sylgard 184 mould	[4]
Ink-jetting technique	Acrylic-based component liquid (1.51)	MLAs	- Controlled shape and radius of lens curvature by the morphology of ZnO NPs surface - Used as antireflection coating in MLAs with ZnO NPs surface	[19]
Inkjet-printing technique	Sylgard 184 (1.42)	Plano-convex lens	- Controlled focal length by varying the droplet volume and surface temperature - Fabricated a flat plano-convex lens with negligible curvature Used the Sylgard 184 plano-convex lens as the smartphone microscope.	[16]

Table 2.1 Lists of fabrication techniques (Continues)

Fabrication techniques	Material (Refractive index)	Type of lens	Distinctive points	Ref.
Needle moving technique	Sylgard 184 (1.42)	Aspheric lens	- Controlled focal length and magnification by varies volume of polymer between 10-200 μl on flat base and change of fabrication temperature - Controlled radius of lens curvature that is ratio of radius of lens and radius of base, by speed moving of needle and the depth of needle position inside the liquid polymer - Designed flat base for handle due to ease of handle - Used polymeric lens as external lens with smartphone became smartphone microscope	[21]

Table 2.1 Lists of fabrication techniques (Continues)

Fabrication techniques	Material (Refractive index)	Type of lens	Distinctive points	Ref.
confined ink-jetting technique	Acrylic-based component liquid (1.51)	Acrylic-based component liquid (1.51)	- Designed Sylgard 184 substrates pattern to form MLAs with lens diameter 100 μm - Controlled the numerical aperture (NA) by volume of polymer on SYLGARD 184 platform MLAs	[34]
confine sessile drop technique	Sylgard 184 (1.42)	Plano-convex lens	- Controlled shape and size by volume of the liquid polymer and diameter of substrate, which effects to lens parameters as focal length, lens curvature, and magnification - Used the Sylgard 184 plano-convex lens as the smartphone microscope.	[17]

2.2 Polymers for lens fabrication

Polymers have many distinctive advantages, such as high transparent, high refractive index, high resistance chemicals and thermals, some flexibility, easy manufacture, and easy peel off mould. For the polymers used in lens fabrication, the refractive index of polymer is the important property that is concerned. The refractive index affects the lens properties explained by the lens maker's equation (see equation 2.3). Accordingly, they are more suitable materials that available fabricated lens.

2.2.1   Polydimethylsiloxane (Sylgard 184)

Polydimethylsiloxane (Sylgard 184) is an optically transparent polymer that is clear, inert, non-toxic, non-flammable, low polarity, low electrical conductivity, and elasticity. The Sylgard 184 also has low surface energy, good chemical and thermal stability, and good insulating properties, thus it was widely used in many applications such as stationary phase in gas-liquid chromatography (GLC) [36], LED Lighting encapsulation [37], and manufacturing of lab-on-a-chip (LOC) devices [38].

The chemical structure of Sylgard 184 consists of silicon (Si), carbon (C), hydrogen (H), and oxygen (O). It has a flexible backbone which is a siloxane (Si-O) molecules as and a repeating unit which is two methyl groups (CH_3) linkage with Si in term $[Si(CH_3)_2O]_n$, [39, 40] as shown in Figure 2.1.

$$\left[\begin{array}{c} CH_3 \\ | \\ -Si-O- \\ | \\ CH_3 \end{array}\right]_n$$
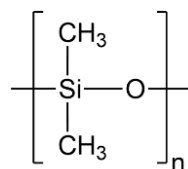
Figure 2.1 Chemical structure of Sylgard 184 where n is the number of unit repetitions

In general, Sylgard 184 has two mixing parts which are base and curing agent. Sylgard 184 base and its curing agent are hydrogen or methyl terminated ends and vinyl terminated ends, respectively (see Figure 2.3). When Sylgard 184 base and curing agent combined, they undergo polymerization *via* organometallic cross-linking reaction with a platinum-based catalyst. Sylgard 184 is polymerization at room temperature (~25°C) for 48 [41-43]. It can reduce cure time by increasing temperature and also avoid bubbles occurred inside the liquid polymer [41]. After polymerization, Sylgard 184 forms Si-CH_2-CH_2-Si linkage which is crosslink through both of terminated ends. The polymerization of Sylgard 184 increases that means more length and more crosslink. Consequently, the higher the amount of crossing, the mixture becomes more viscosity. The viscosity was reached infinite until Sylgard 184 convert from a liquid to an elastic solid. The mixture becomes a hundred percent product without waste after polymerization [39, 44, 45].
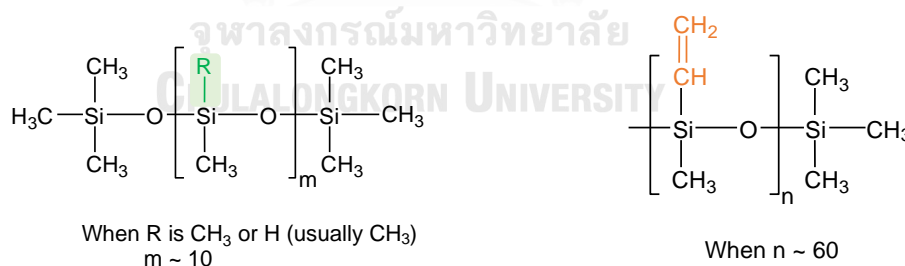
Figure 2.2 The chemical structure of (A) Sylgard 184 base and (B) Sylgard 184 curing agent where m and n are the number of unit repetitions and approximately equals ~ 10 and ~ 60, respectively.
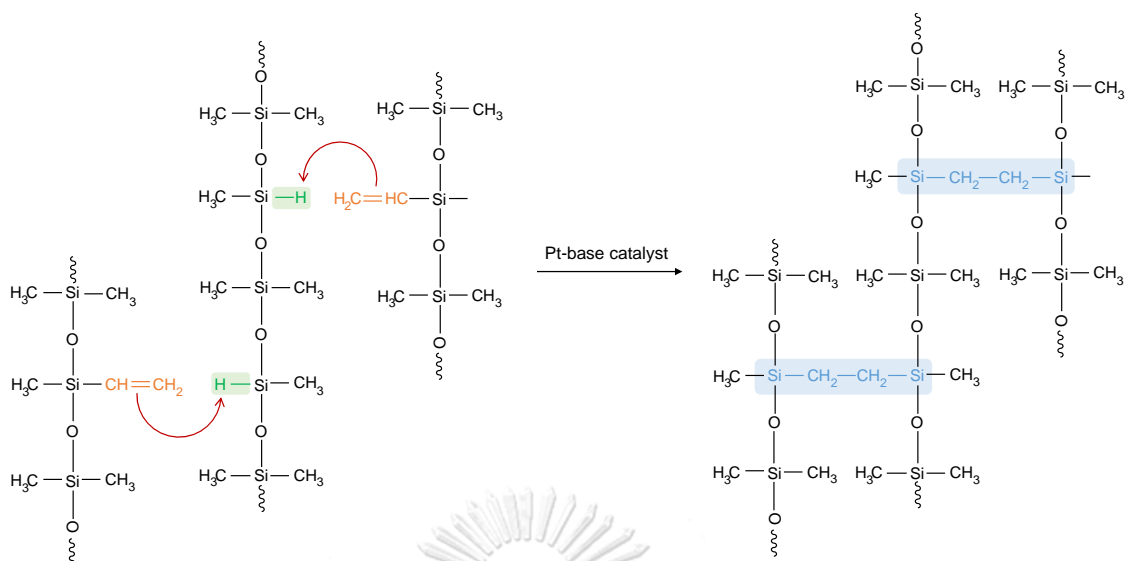
Figure 2.3 The organometallic cross-linking reaction of Sylgard 184 at room temperature with the platinum-based catalyst inside of Sylgard 184 curing agent solution.

2.2.2 Norland Optical Adhesive 61 (NOA 61)

Norland Optical Adhesive 61 (NOA 61) is ultraviolet (UV) – curable adhesive polymer whit clear color. Although the chemical structure of NOA 61 is unclarified by the manufacturer, however the X-ray photoelectron spectroscopy (XPS) of NOA 61 indicated that the component elements of NOA 61 consist of C (68.5 at, %), O (23.3 at, %), Si (5.7 at, %), N (1.8 at, %), and S (0.7 at, %) [46]. Nevertheless, the change of molecular information of NOA 61 before and after polymerization were also monitored by Raman spectroscopy [47] and Attenuated total reflection Fourier transform infrared spectroscopy (FTIR) [46]. The aromatic ring vibration at 1604 cm$^-$^{1}, thiol (S-H) group at 2582 cm^{-1}, vinyl (C=C) group at 1650 cm^{-1}, carbonyl (C=O) group of carboxyl (COOR) at 1746 and 1764 cm^{-1} presented in the liquid polymer before curing. The absent of thiol (S-H), vinyl (C=C) and allyl (CH$_2$-CH=CH$_2$) group indicate the completely crosslink of the polymer [46, 47]. The results suggested that the chemical structure of NOA 61 is based on multifunctional thiolenes that undergo the thiol–ene photopolymerization under UV-irradiation.

The NOA 61 is a thiol-ene polymer which was polymerization under UV light exposure as well as the photochemical process. The thiol-ene polymer is a part of a liquid that consists of monomers with thiol functional group (R-SH), monomers with allyl functional group (R'-CH$_2$-CH=CH$_2$) and photoinitiators [48-50]. The photoinitiators are small molecules. When the photoinitiators are exposed to UV light, they are excited and generated active molecules to form bonding with monomers and oligomers until the liquid polymer became harden to solid polymer (Figure 2.4).

Thiol-ene photopolymerization
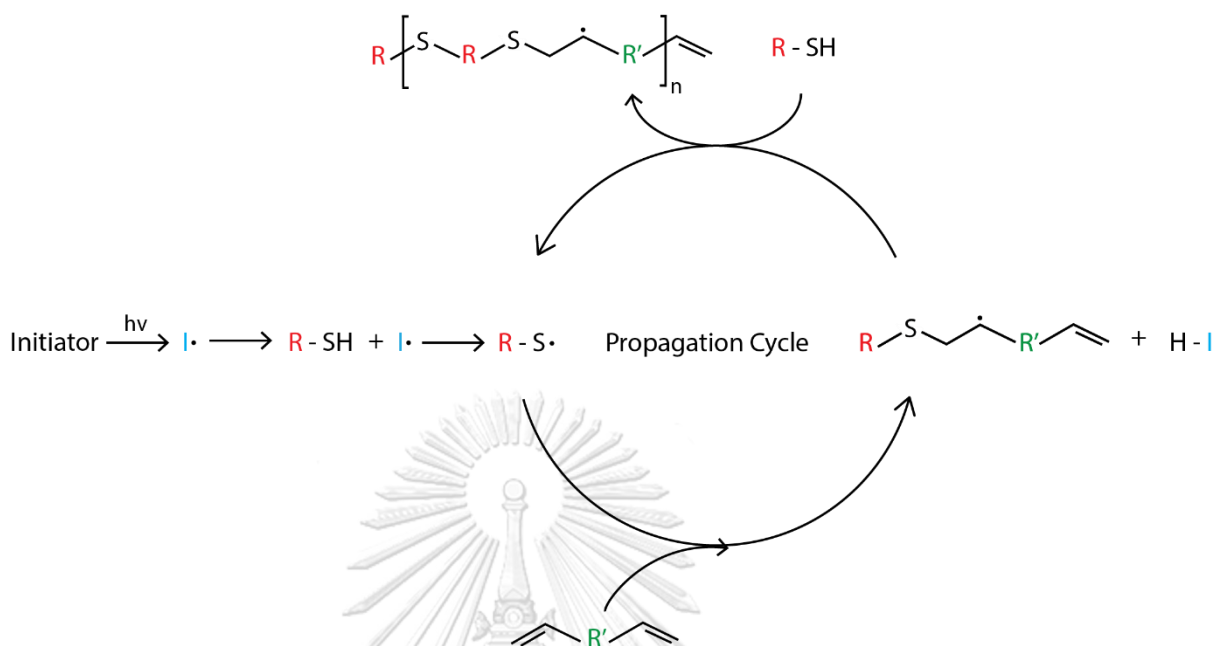
Figure 2.4 Reaction mechanism of thiol-ene photopolymerization

The curing of NOA 61 is accomplished after 10-15 min photopolymerization under ultraviolet light (UV) exposure at a wavelength of 350-380 nm. The recommended UV-light source for fully curing is 3 Joules/cm^2 (a 100-watt mercury lamp at 6" height) [51]. The oxygen does not affect polymerization. In addition, the controllable factor of light source influences the curing time, including, power, intensity, and energy. Hence, the curing time can be reduced if the light source is low power, low intensity, and low energy. The advantages of NOA 61 are solid with slight flexibility, high refractive index (n ~1.56), excellent clarity, and low shrinkage. These properties are important for design high-quality optical elements. The NOA 61 is recommended for adhering with glass surfaces, metals, fiberglass, lenses, prisms and mirrors for splicing optical fibers.

Table 2.2 Physical properties of Sylgard 184 and NOA 61

Properties	Sylgard 184	Ref.	NOA 61	Ref.
Color	Colorless	[42]	Colorless	[51]
Refractive index @ 632.8 nm (Solids)	1.42	[42]	1.56	[51]
Viscosity at 25 °C (cps)	5100	[42]	300	[51]
Density (kg/m^3)	0.956	[52]	1,290	[51]
Surface tension (dyne/cm)	20-23	[17]	40.0	[51]
Dielectric Strength (volts/mil)	500	[42]	980	[51]
Volume Resistivity ($\Omega \cdot$ cm)	2.9 x 10^{14}	[42]	1.0	[51]
Curing method	Thermal cured 80 °C, 30 min	[42]	UV cured 350-380 nm (100 watt), 15 min	[51]

จุฬาลงกรณ์มหาวิทยาลัย

CHULALONGKORN UNIVERSITY

2.3 Polymeric plano-convex lens

Most of the polymeric lens fabrications are plano-convex lens. The plano-convex lens consists of one flat surface and one convex surface that is a part of spherical shape. There are lens diameter $\emptyset$, radius of lens r, height of lens H, radius of lens curvature R, , refractive index of lens material n, contact angle θ, and focus point C, as shown in figure 2.1
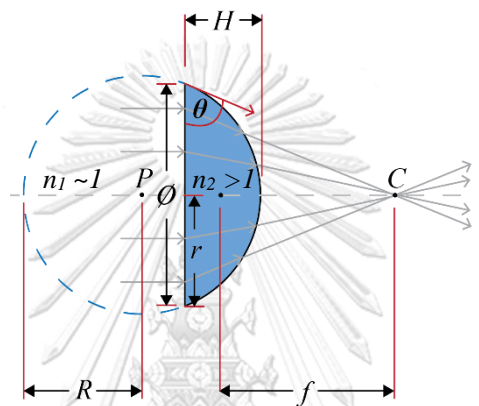
Figure 2.5 Ray tracing of the plano-convex lens.

Figure 2.1 shown the incident lights pass air ($n_1 \sim 1$), and then enter the plano-convex lens which fabricated from polymer ($n_2 > 1$). The incident light which passed the intermedia between air and the polymeric lens, refracted under an angle between the incident lights and the polymeric lens. The refracted lights also were refracted again under an angle between the plano-convex lens and air, before diverging towards at the one point which is focus point, C. The distance from planar side of the plano-convex lens to focus point is the focal length. It described the relationship about the radius of lens curvature R, the height of lens H, and the radius of lens r, can be followed by equation 2.1 as [53]:

$$R = (K + 1)(\frac{H}{2} + \frac{r^2}{2H})$$ (2.1)

Where K is the aspherical constant. When aspherical constant K is equal zero, it means the plano-convex lens is a perfectly spherical shape which neglects gravitational force. Accordingly, the radius of lens curvature R equals the radius of lens r. It solved the relative between R, H, and contact angle of lens (θ) is given by [27, 54]:

$$\cos \theta = \frac{(R - H)}{R}$$ (2.2)

In addition, the focal length f is the shortest distance between the planar side of the plano-convex lens and focus point, C. The focal length f of the thin lens was relationship with the radius of lens curvature R and the refractive index of lens materials n_1, by following Len's maker equation as [27, 53]:

$$\frac{1}{f} = (n_2 - 1)(\frac{1}{R_2} - \frac{1}{R_1})$$ (2.3)

Where f is the focal length, n_2 is the refractive index, R_1 and R_2 are the radius of lens curvature in flat side and convex side, respectively. The R_1 of the plano-convex lens is infinite, thus $\frac{1}{R_1}$ approximately equals zero. The focal length f of the plano-convex lens is given by [53]:

$$f = \frac{R}{n_2 - 1}$$ (2.4)

2.4 Surface plasmon resonance (SPR)

Surface plasmon resonance (SPR) sensor is a promising optical sensor that has high selectivity and sensitivity against the change of local refractive index caused by affinity interactions of a variety of molecules. Due to its available detection of refractive index variation (*n*) in real-time monitoring and without any labeling, SPR is most of attracted attention for detection and analysis of biological/chemical interactions in many fields, such as food industry [55], environmental monitoring [56], and biomedical [57, 58].

The basic principle of SPR is founded on a physical optics phenomenon that observed when p-polarized light, named incident light, passed through a prism and collided with a thin metal film under total internal reflection conditions (TIR) conditions. The incident light was coupling into a prism and penetrated into metal-dielectric interface. When all of the incident light is totally reflected at a critical angle (θ_c), it provided attenuated total reflection. When the incident light is illuminated from a prism (medium denser) into a dielectric surface (thinner denser), it generated evanescent wave which has a depth of half the wavelength and then gets back to a denser medium. While the free oscillating electron on the metal surface was excited by incident light, it penetrated into metal-dielectric interface resulting in the surface plasmon waves that propagates parallel along the metal surface. When the momentum of evanescent wave and surface plasmon waves matched, SPR is excited. The reflection spectrum decreased due to the transfer of energy from evanescent waves to surface plasmon, resulting in the appearance of SPR dip angle (Figure 2.6) [55, 58]. The reflected spectrum can be tracked in angle, wavelength, intensity or phase modulation [59].

The SPR dip angle depends on many factors, such as the optical properties of prism, metal film thickness, the wavelength of the incident light and the local refractive index of the dielectric medium [60]. A conventional SPR base on the Krestchmann configuration, are used to increase the momentum of incident light by using a high refractive index prism [61, 62]. The metal films on SPR sensor can use silver, gold, and aluminum. Most satisfying metal is made from gold due to excellent surface stability, and resistant to oxidation and contaminants [63]. In addition, the light source can select suitable a function spectrum. It should be a monochromatic light and p-polarized to gain a sharp dip [64]. When the metal films and the incident light are constant, the shift of SPR dips is changed that following the change of the local refractive index of the dielectric medium.
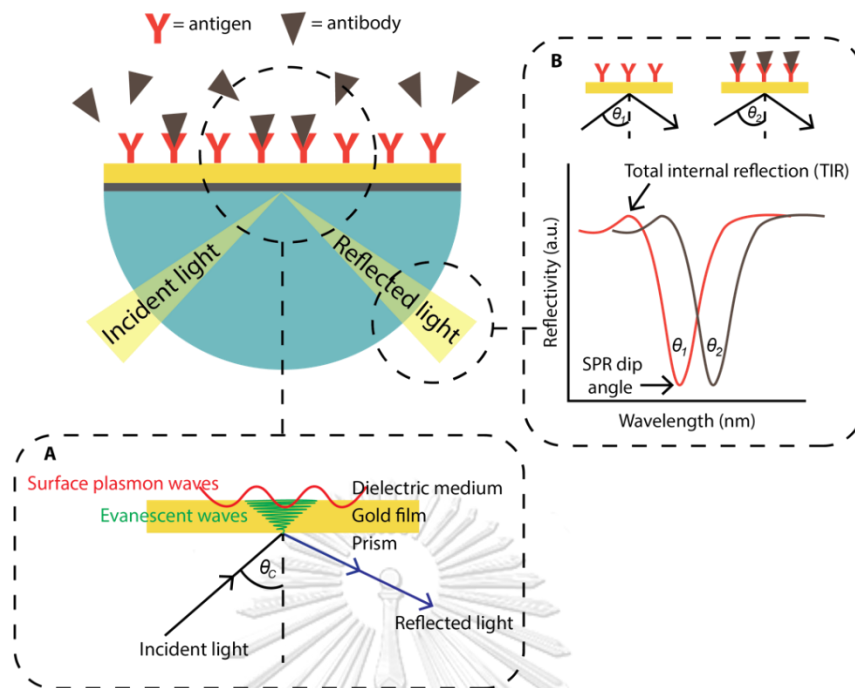
Figure 2.6 Principle of SPR sensor base on Kretschmann configuration under TIR condition. (A) The relative of three-layer geometer for exciting SPR. (B) The reflected spectrums were following the change of refractive index of dielectric medium, as antigen and antibody, that monitoring SPR dip angle by wavelength modulation.

CHARTER III

EXPERIMENTAL SECTION

3.1 Materials and Chemical Reagents

Polydimethylsiloxane (PDMS, Sylgard 184) was purchased from Dow Corning Co., Ltd (USA). Norland optical adhesive 61 (NOA 61) was purchased from Norland products Inc (USA). A certified refractive index liquids series: type A with a refractive index of 1.592 ±0.002 was purchased from Cargille Laboratories Inc (USA). Ethylene glycol was purchased from Kanto Chemical Co., Inc (Japan). 1,8-Octanedithiol (ODT) and dichloromethane were purchased from Sigma-Aldrich Inc (USA). All chemicals have structure and unique optical properties. The 1951 USAF pattern resolution target with resolution from group 2 to group 7 and 6 elements per group was purchased form Thorlabs Inc (USA).

3.2 Fabrication of plano-convex lens

The fabrication of plano-convex lenses consists of the following steps as (1) preparation of lens substrates, (2) fabrication of plano-convex lens with Sylgard 184 and NOA 61.

3.2.1 Preparation of lens substrates

3.2.1.1 Preparation of PMMA circular disks

To prepare polymethylmethacrylate (PMMA) circular disks, the 1 mm-thick flat PMMA sheet with a surface roughness (R_a) ~2 nm was cut into circular disks with diameters of 2.5-6 mm by using a laser cutter (TB-1490, T-BROS Laser Engineering Co., LTD). The PMMA circular disks were cleaned under sonication with liquid detergent for 15 minutes, following with DI water twice for 15 minutes. After that, cleaned-circular disks were kept in a dust-free desiccator until use. Figure 3.1 illustrates a various size of PMMA circular disks.
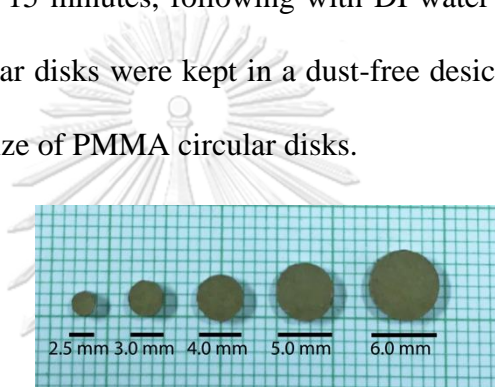
Figure 3.1 A photographic image of PMMA circular disks with diameters of 2.5, 3.0, 4.0, 5.0 and 6.0 mm

3.2.1.2 Preparation of Sylgard 184 circular disks

Sylgard 184 precursor was prepared by mixing of the Sylgard 184 base and its curing agent in a ratio of 10:1 %w/w. The Sylgard 184 precursor was degassed in a vacuum desiccator until the residue air bubbles were completely removed. Then, the Sylgard 184 precursor filled in the prepared acrylic molds with 60 x 60 cm^2. It was left overnight undisturbed at room temperature (~30 ^{o}C) for curing the Sylgard 184 precursor and obtained transparent elastomeric Sylgard 184 films (Sylgard 184 films) with the thickness of 0.6 mm. After that, the Sylgard 184 films were punched in various diameter size by using hollow punchers (2.5, 3.0, 4.0, 5.0 and 6.0 mm in

diameter) to prepare the Sylgard 184 circular disks. The Sylgard 184 circular disks were kept in a dust-free desiccator until use. Figure 3.2 illustrates a various of Sylgard 184 circular disks.
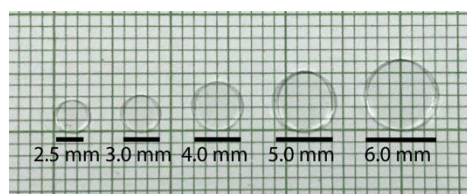
Figure 3.2 Photographic image of (A) the Sylgard 184 circular disks with diameter 2.5, 3.0, 4.0, 5.0 and 6.0 mm.

3.2.2 Fabrication of plano-convex lens

To fabricate plano-convex lenses, the Sylgard 184 precursor and liquid NOA 61 were dispensed on the 1 mm-thick PMMA and the ~0.6 mm-thick Sylgard 184 circular disks as prepared in 3.2.1, respectively. The lens substrates were attached on a clean glass slide. The liquid polymers spread until reaching the edge of the lens substrates. The contact angle at the edge of the fabricated lens was controllable by adjusting the weight of liquid polymer droplet. It was left undisturbed for at least 5 min to form a stable spherical cap before curing. The lens fabricated from Sylgard 184 and NOA 61 were cured by thermal curing at 80 °C for 30 min and UV photocuring ($\lambda = 350\text{-}380$ nm) for 6-8 hours, respectively (as shown on Figure 3.3).

A: Sylgard 184 plano-convex lens

B: NOA 61 plano-convex lens
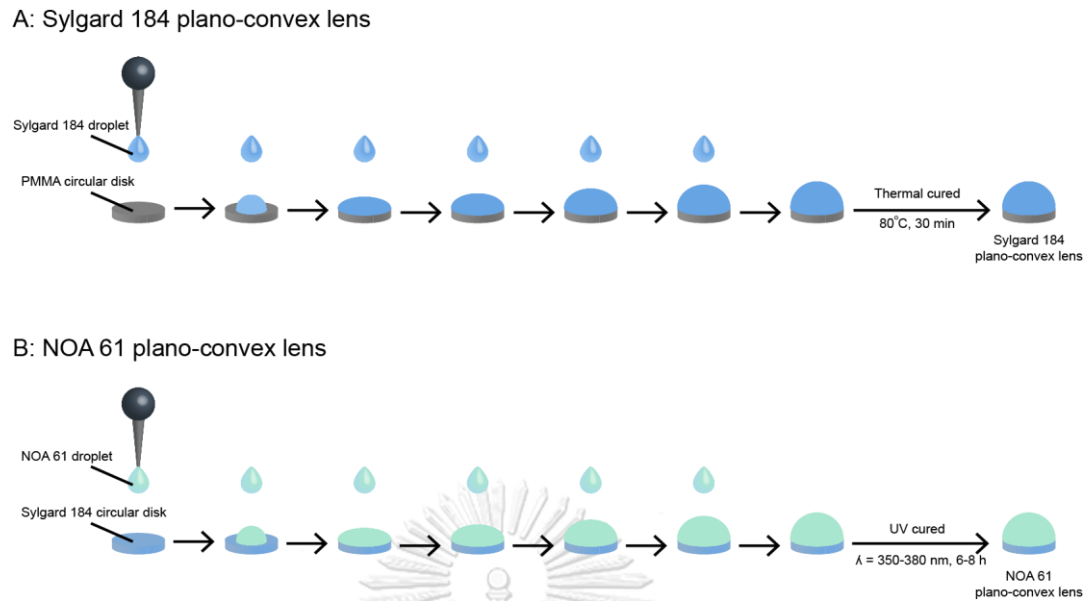
Figure 3.3 The fabrication of (A) Sylgard 184 and (B) NOA 61 plano-convex lens by confined sessile drop technique.

3.3 Lens characterizations

3.3.1 Contact angle and lens envelop measurement

To measure the value of contact angle and lens envelop of the fabricated lens, we took a digital macro photograph of the fabricated lens and analyzed the value of contact angle and envelop using an image analysis program. The plano-convex lens, which was removed from the lens substrate, was set on a home-made macro photographic set-up. The set-up should be arranging from a LED light source with a diffuser, adjustable stage and digital camera (Nikon D90) with a macro lens (AF-S VR Micro-NIKKOR 105mm f/2.8G IF-ED). The home-made macro photographic setup is shown in Figure 3.5. The value of contact angle and lens envelop of the fabricated lens were evaluated from the macro photograph (Figure 3.4 (B)) by using ImageJ software with Java-based image processing developed by National Institutes of Health, USA), along with a dropsnake plug-in (based on ImageJ software).
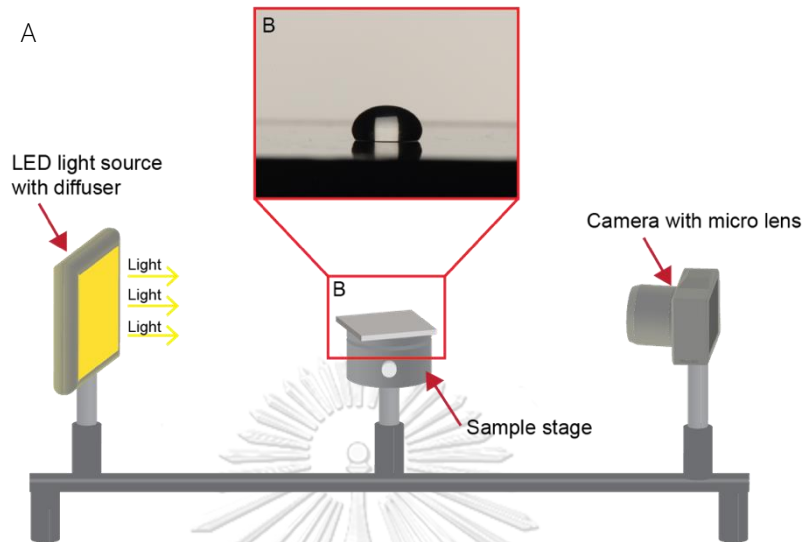
Figure 3.4 (A) Schematic drawing of the home-made macro photographic setup. (B) the image of 4-mm NOA 61 plano-convex lens without Sylgard 184 circular substrates.

3.3.2　Focal length measurement

The focal length of the fabricated lens was measured by using a focal length measurement kit (Lens and Smart Classroom Co., Ltd., Thailand). The focal length is the shortest distance in millimeter (mm) unit between the objective and the curve of plano-convex lens. The focal length measurement was set-up by from placing the green LED light at the zero point. Next, the fabricated lens was mounted onto the lens holder parallelizing to the LED light at the distance of 20 cm. The focusing screen was placed at the back of the lens holder and then adjusted the position to find the sharpest green point on the focusing screen. The focal length of the lens was calculated from the distance between the lens holder and the focusing screen. The

focal length measurement using the focal length measurement kit is plausible. This is due to it has been already standardized with the Flatness interferometer (model Fujinon and type F601).
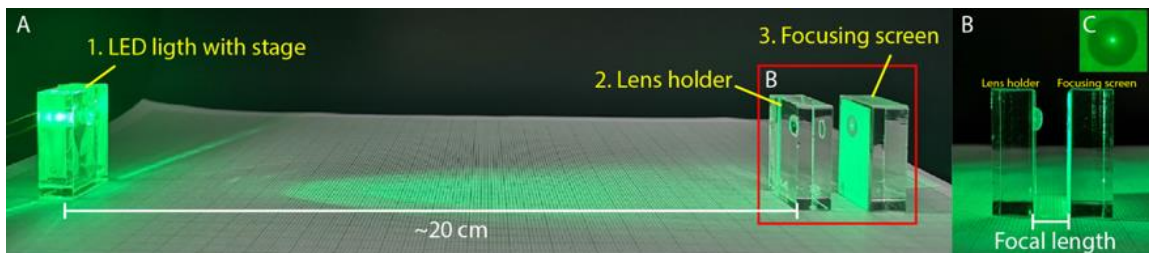
Figure 3.5 (A) Side view of the focal length measurement kit includes LED light, plano-convex lens with lens holder and focusing screen. (B) The distance between the lens holder and the focusing screen is using for calculation of the focal length. (C) the sharpest green spot on the screen at the focal point.

3.3.3 Magnification

Magnification (M) of the plano-convex lenses is related to the focal length as described in equation 3.1

$$M = \frac{250}{f} \tag{3.1}$$

Where M is the magnification of the plano-convex lenses

f is the focal length (mm) of the plano-convex lenses

3.3.4 Resolution and contrast

To demonstrate and compare the performance of the fabricated lens for using in smartphone microscope, the fabricated lenses (Sylgard 184 and NOA 61 plano-convex lens) and optical microscope (Carl Zeiss: Axio Scope.A1) with the same magnification (50x) were compared using the combined resolution and distortion test targets under illumination from the same illuminaton unit (Carl Zeiss: Axio Scope.A1). The Sylgard 184 plano-convex lens was directly attached to the center of the smartphone camera (Huawei P20 pro). Meanwhile, NOA 61 plano-convex lens was attached to the smartphone camera using a drop of certified refractive index liquids without any air gaps and bubbles, as shown on Figure 3.6. In addition, the 5x objective lens of the optical microscope was used to compare the lens quality against the polymeric lens. The sample is 1951 USAF resolution or permanent glass slide
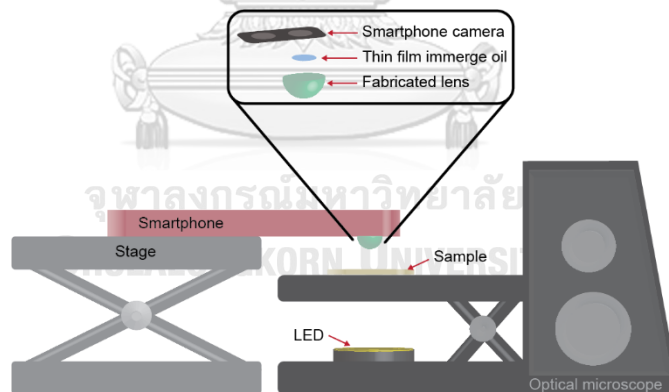
Figure 3.6 Schematic presents resolution and percent contrast test set-up

The combined resolution and distortion test target in negative versions (black target) consist of a 1951 USAF patterns (Groups 2 – 7), a sector star (36 Bars through 360°), concentric circles, grids (100 µm, 50 µm, and 10 µm), and Ronchi rulings (30 - 150 lp/mm). The target features are useful for testing resolution, field distortion, focus errors, and astigmatism. In this work, we focus on the 1951 USAF patterns. The 1951 USAF patterns are used for measuring the image resolution. It consists of groups number labeled 2 to 7 on the top, and element number labeled 1 to 6 per group number on the sides. Each element has equally spaced bars; three horizontals and three verticals (Figure 3.7). The 1951 USAF patterns were taken with the fabricated lens and measured the resolution and percent contrast through inspect the ability to separate the horizontal and the vertical bars. The smallest group number and element number is acceptable which is the horizontal and the vertical bars can still be recognized as three distinct bars and percent contrast more than 20 percentages. By increased group number and element number are progressively produced smaller bars. If it can recognize, it has high resolution.
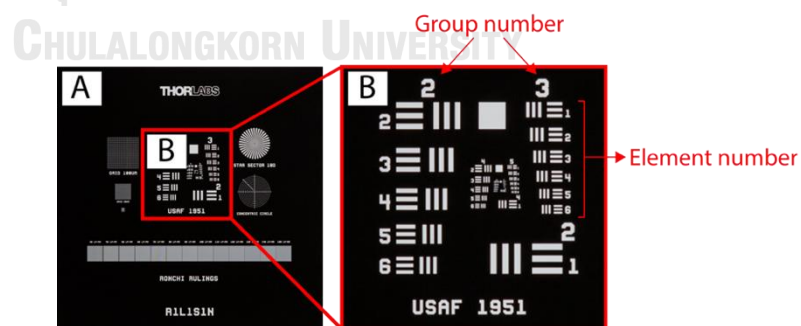
Figure 3.7 (A) Photograph of the combined resolution and distortion test target in negative versions (black target) and (B) the enlargement of a standard USAF Resolving Power Test Target 1951.

3.4 Smartphone microscope application

To investigate the application of the polymeric plano-convex lenses as an objective lens for smartphone microscope, we demonstrate the observing of the display of Huawei P20 pro, all instruments were set as same as reported in 3.3.4. We compare the quality image of target resolution at the same magnification during optical microscope and the fabricated lens as Sylgard 184 plano-convex lens and NOA 61 plano-convex lens.

3.5 Fabricated SPR sensor chip fabricaiton

3.5.1 Preparation of miniature SPR sensor chip

We further demonstrated the utilization of the polymeric plano-convex lens as an optics for SPR application. The miniature SPR sensor chip based on the Kretschmann configuration was fabricated by deposited a 3-nm Cr and a 47-nm Au films on the planar side of the polymeric plano-convex lens *via* thermal evaporation (Figure 3.7). Then, the fabricated SPR sensor chip was attached on the mounting slot of a 3D-printed flow cell by using liquid NOA 61 as a glue. After curing under UV irradiation, the miniature SPR sensor chip was securely mounted and the miniature SPR flow cell was obtained (Figure 3.8).
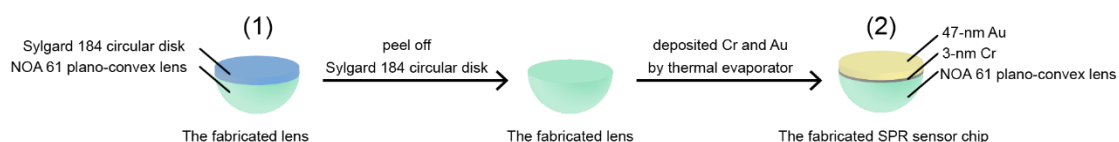
Figure 3.8 SPR sensor chip fabrication from 6-mm NOA 61 plano-convex lens.
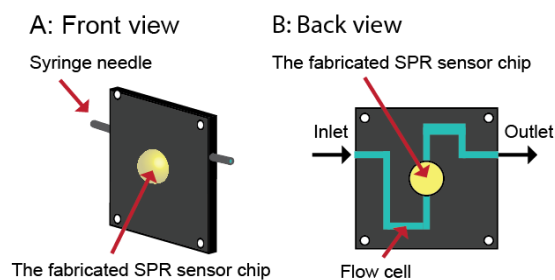
Figure 3.9 Schematic drawing (A) front view and (B) back view of the fabricated SPR sensor chip. The flow cell was designed by a computer-aided design (CAD) software and printed out by a high-performance 3D printer (Ultimaker 3, Ultimaker B.V., Netherlands).

3.5.2   Fabrication of SPR sensor chip for H_2O_2 detection

The SPR sensor chip was soaked in a 5 mM 1, 8-Octanedithiol (ODT) which was dissolved in ethanol for 16 h. After rinsing with DI water, the sensor chip was soaked in an aqueous solution of 20 mM silver nanoparticles (AgNPs) for 6 h (Figure 3.9). Then, the SPR sensor chip was rinsing with DI water, the PR sensor chip was ready for H_2O_2 detection. For the developed sensor chips, ODT performed as the linker between gold film and AgNPs. The present of H_2O_2 in the system lead to the decomposition of AgNPs which cause the shift of the SPR dip peak.
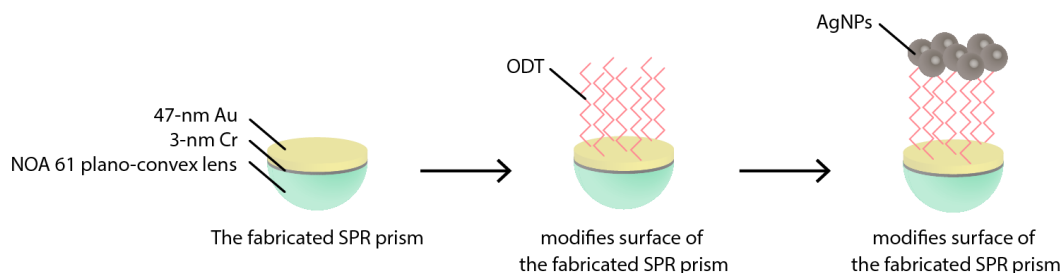
Figure 3.10 Schematic illustrated the deposition of silver nanoparticles (AgNPs) on the surface of SPR sensor chip. 1, 8-Octanedithiol (ODT) was utilized as the linker between gold surface and AgNPs.

3.5.3 Home-built SPR set up

The wavelength-modulated SPR characterization was performed by using a home-built SPR unit (Figure 3.11). The white light from a halogen source (HL-2000, Ocean Optics) passed through a 600 μm optical fiber (F600-UVVis-SR, StellarNet Inc) to a collimating lens (74-VIS, Ocean Optics). The light beam passed through a linear polarizer, an optical aperture (diameter, 0.7 mm), and a biconvex lens with a focal length of 150 mm, respectively, in order to collimate light before reaching a SPR sensor chip which mounted on a θ-2θ motorized goniometer. A plano-convex lens with a focal length of 12 mm and a collimating lens (74-VIS, Ocean Optics) collected the reflected light into a 600 μm optical fiber (F600-UVVis-SR, StellarNet Inc) Then, the reflected light is measured by using a UV−vis spectrometer (USB 4000, Ocean Optics).
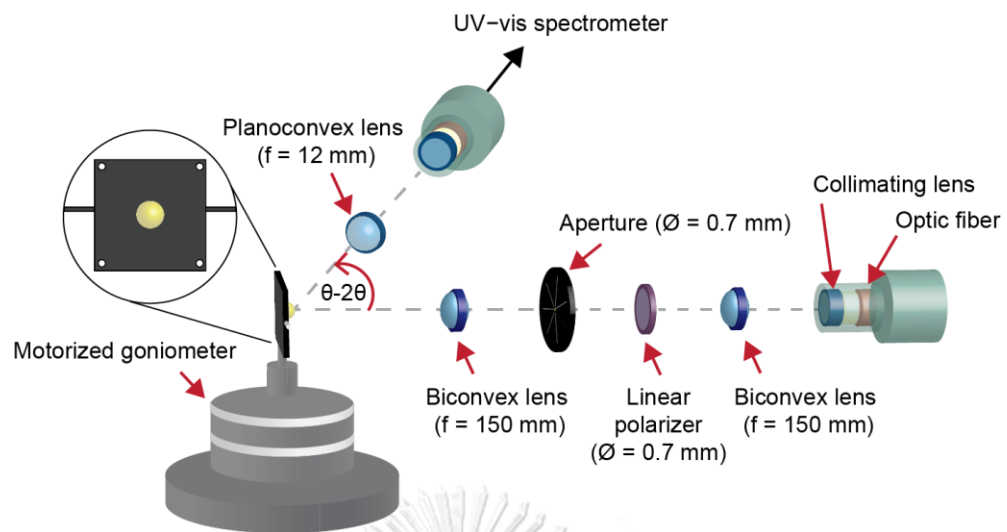
Figure 3.11 Schematic drawing of the home-built SPR unit

CHARTER IV

RESULTS AND DISCUSSION

4.1 Fabrication polymeric plano-convex lens

To fabricate a polymeric plano-convex lens using Sylgard 184 and NO61, we employed the confined sessile drop technique due to the ability of controllable lens geometry. The polymer droplets were dropped on the circular lens substrates made from PMMA and Sylgard 184, respectively. The liquid polymer gradually spread and radially expanded over the surface of the circular disk as a spherical cap. When the three-phase contact line (polymer droplet/Air/circular disk) is always free expanded along the contiguous surface until it was pinning at the edge. After the polymer droplets reached the sharp edge of the lens substrate, it eventually stopped spreading and pinning at the edge of a circular disk with a contact angle (θ). In essence, the confine sessile drop technique precisely controlled θ through polymer droplets, which dropped on the lens substrate. The liquid polymer can be added/removed from the droplets to gain the spherical cap with various θ. In this case, θ for polymer droplets at the edge is described by Gibbs inequality equation as following [17, 65, 66]:

$$\theta_c = \theta_e + (180 + \phi) \tag{4.1}$$

Where θ_c is critical contact angle, θ_e is equilibrium contact angle on the flat surface without the edge, and ϕ is the subtended angle at the edge (in this case, ϕ is equal 90°). Another meaning of θ_c is the maximum contact angle of the spherical cap before droplets flow across the sharp edge of circular disk. Consequently, additional polymer droplets can increase as long as θ is smaller than θ_c.

4.1.1   Equilibrium contact angle (θ_e) and critical contact angle (θ_c)

To estimate θ_c from Gibb's inequality equation in equation 4.1, the value of θ_e must be evaluated. In our experiment, we fabricated Sylgard 184 plano-convex lens on PMMA circular disks and NOA 61 plano-convex lens on Sylgard 184 circular disks. When the Sylgard 184 droplets were dropped on the PMMA sheet, the value of the initial θ was dramatically decreased by time. The result clearly shows that the change of θ value stops at 24 h, suggesting the spreading of liquid polymer already reaches the equilibrium state, Figure 4.1(A), and (C). Thus, the value of θ_c of the Sylgard 184 droplets on PMMA sheet derived from equation 4.1 equals 90°. For the NOA 61 droplets on the Sylgard 184 sheet, the value of θ quickly changed after dispensing of the polymer onto the surface of Sylgard 184. After 24 h passed, it did not form a thin film, but a spherical cap of NOA 61 on Sylgard 184 film with the θ_e value of 50° (Figure 4.1(B) and (C)). Thus, the value of θ_c of NOA 61 droplets on Sylgard 184 film devised from equation 4.1 equals 140°. According to Gibb's inequality equation, the value of, θ_e for Sylgard 184 droplets on PMMA circular disk and NOA 61 droplets on Sylgard 184 circular disk are 90° and 140°, respectively. Rising the contact angle of three-phase contact line (polymer droplet/Air/circular disk) above θ_e cause the flow of liquid polymer over the edge of the circular disk.

A: Sylgard 184 droplet on 1 mm-PMMA sheet without edge
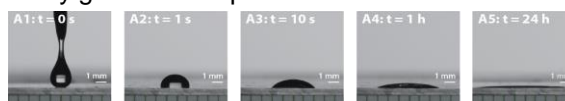
B: NOA 61 droplet on Sylgard 184 film without edge

C: Time dependent of contact angle
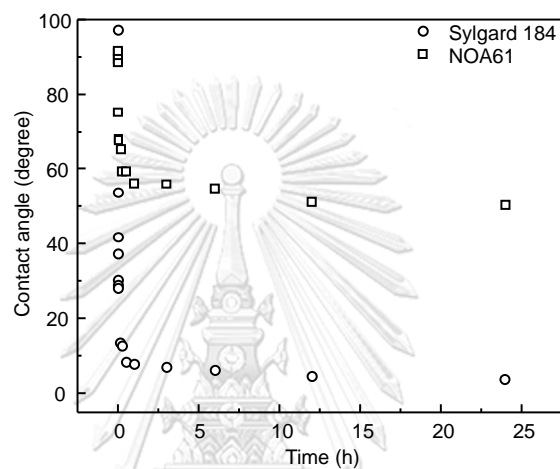
Figure 4.1 Optical images of (A) 3.5-mg Sylgard 184 and (B) 8.8-mg NOA 61 droplets on flat surface. (C) Both of liquid polymers were spread by time until reaching equilibrium state where the contact angle was not changed and exposed the equilibrium contact angle.

4.1.2   Polymeric plano-convex lens formation

The confined sessile drop technique can precisely control the lens geometry by the dispense of liquid polymer on the lens substrate. The amount of liquid polymer dispensed on the lens substrate was adjusted though the weight of the liquid polymer. To observe the difference of focal length that is affected by the changed lens geometry, such as, contact angle (θ), and lens diameter ($\emptyset$), we fabricated the lens with different value of θ by changing of the weight of liquid polymer disperse on the 4.0 mm diameter of the lens substrates. We observed that the increase of liquid polymer amount causes the increase of contact angle. The amounts of liquid Sylgard 184 ranging from 2.8 ± 0.11 mg to 17.9 ± 0.16 mg produced the Sylgard 184 droplets with the corresponded value of θ from 20.50 ± 1.32 degrees to 90.31 ± 0.84 degrees, respectively (Figure 4.2 (A), and Table 4.1). When the amount of liquid Sylgard 184 increases more than 17.9 ± 0.16 mg, the hemispherical droplet collapsed because of the liquid polymer flow over the edge of the lens substrate. In the case of NOA 61, the increased of the weight of NOA 61 from 8.5 ± 0.46 mg to 34.7 ± 0.35 mg created the hemispherical droplet on the Sylgard 184 substrates with the corresponded θ from 51.44 ± 0.76 degrees to 120.95 ± 0.51 degrees (Figure 4.2 (B), Table 4.1). After curing, the hemispherical polymer droplets polymerized and become polymeric plano-convex lenses. Since the Sylgard 184 and NOA 61 have low shrinkage, the lens shape retains without significant alteration of the shape (Figure 4.3). we measure the focal length of the lens (f) and calculate the magnification (M) of the lenses, as shown in Figure 4.2 and table 4.1. The result shows that the increase of θ, the decrease of f. meanwhile, decrease of f cause the increase of magnification. The results suggest that the fabrication of polymeric plano-convex lenses with different

lens shapes (different value of θ) can perform by adjusting the weight of the liquid polymer. This is useful for large scale production where the speed and quality of production are essential.
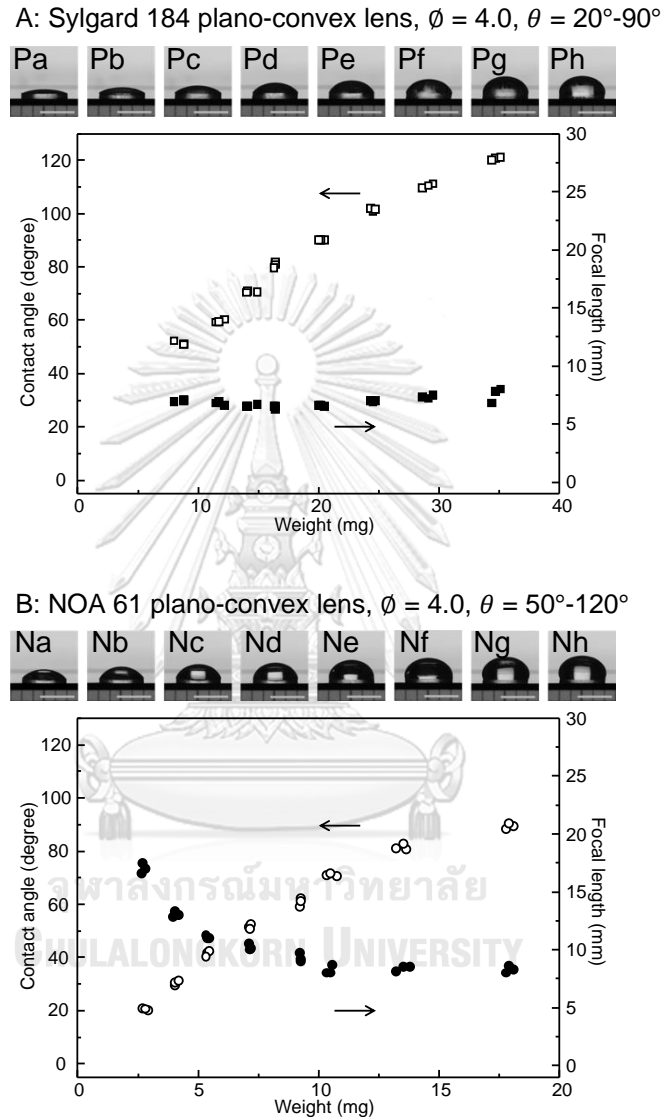
Figure 4.2 The relationship of the weight of liquid polymer with the contact angle (θ) and the focal length (*f*) of (A) Sylgard 184 plano-convex lens and (B) NOA 61 plano-convex lens fabricated by the confined sessile drop technique on the 4.0 mm diameter of lens substrates. The digital photograph of Pa to Ph and Na to Nh were one of lenses at each of the contact angle. Scale bar in the digital photograph (Pa to Ph, and Na to Nh) indicated 3 mm.

Table 4.1 The relationship of the weight of liquid polymer, contact angle (θ), focal length (f), and the magnification (M) of lens fabricated on the 4.0 mm lens substrates.

Polymeric lenses	Lenses	Weight (mg)	Contact angle, θ (°)	Focal length, f (mm)	Magnification, (M)
Sylgard 184 plano-convex lens	Pa	2.8 ± 0.11	20.5 ± 1.32	16.2 ± 1.78	15.4
	Pb	4.1 ± 0.09	30.49 ± 0.46	12.4 ± 1.25	20.1
	Pc	5.4 ± 0.06	41.08 ± 0.64	11.1 ± 0.12	22.6
	Pd	7.1 ± 0.04	51.04 ± 1.38	10.2 ± 0.26	24.5
	Pe	9.3 ± 0.02	59.86 ± 0.77	9.3 ± 0.36	26.9
	Pf	10.6± 0.32	71.11 ± 0.80	8.3 ± 0.58	30.0
	Pg	13.7 ± 0.66	79.97 ± 1.68	8.5 ± 0.40	29.4
	Ph	17.9 ± 0.16	89.31 ± 0.84	8.3 ± 0.30	30.1
NOA 61 plano-convex lens	Na	8.5 ± 0.46	51.44 ± 0.76	7.0 ± 0.10	35.7
	Nb	11.8 ± 0.36	59.63 ± 0.58	6.8 ± 0.15	36.9
	Nc	14.3 ± 0.49	70.70 ± 0.29	6.6 ± 0.12	38.1
	Nd	16.4 ± 0.06	80.72 ± 1.10	6.4 ± 0.12	38.9
	Ne	20.2 ± 0.25	91.18 ± 0.03	6.6 ± 0.06	38.1
	Nf	24.5 ± 0.20	101.35 ± 0.63	7.0 ± 0.06	35.9
	Ng	29.1 ± 0.45	110.36 ± 0.81	7.3 ± 0.15	34.1
	Nh	34.7 ± 0.35	120.95 ± 0.51	7.5 ± 0.64	33.2

จุฬาลงกรณ์มหาวิทยาลัย

CHULALONGKORN UNIVERSITY
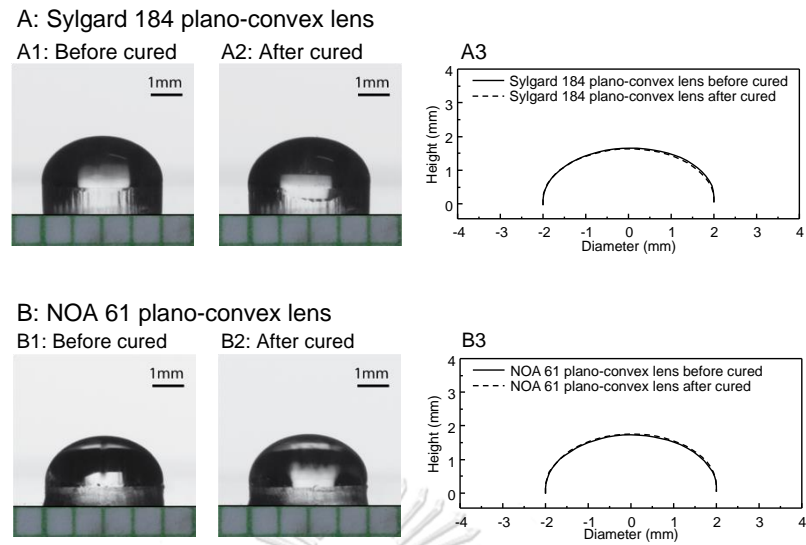
Figure 4.3 Digital photograph of (A) Sylgard 184 and (B) NOA 61 plano-convex lens taken (1) before and (2) after curing. The envelope profiles of (A3) Sylgard 184 and (B3) NOA 61 plano-convex lens before/after curing.

Fabrication of polymeric lens has been conducted for other diameters, including 2.5 mm, 3.0 mm, 5.0 mm, and 6.0 mm. Figure 4.4, Table 4.2 and Figure 4.5, Table 4.3 illustrate the relationship of polymer weight, contact angle (θ), focal length (f), and the magnification (M) for the Sylgard 184 and NOA 61 plano-convex lenses, respectively. Event the diameter of the lens substrate is not 4.0 mm, fabrication of polymeric lenses with different lens parameters can be accomplished by adjusting the weight of the polymer. Similar to the lens with 4.0 mm diameter, we still observed that the increase of θ cause the decrease of f. While the decrease of f causes the increase of magnification.
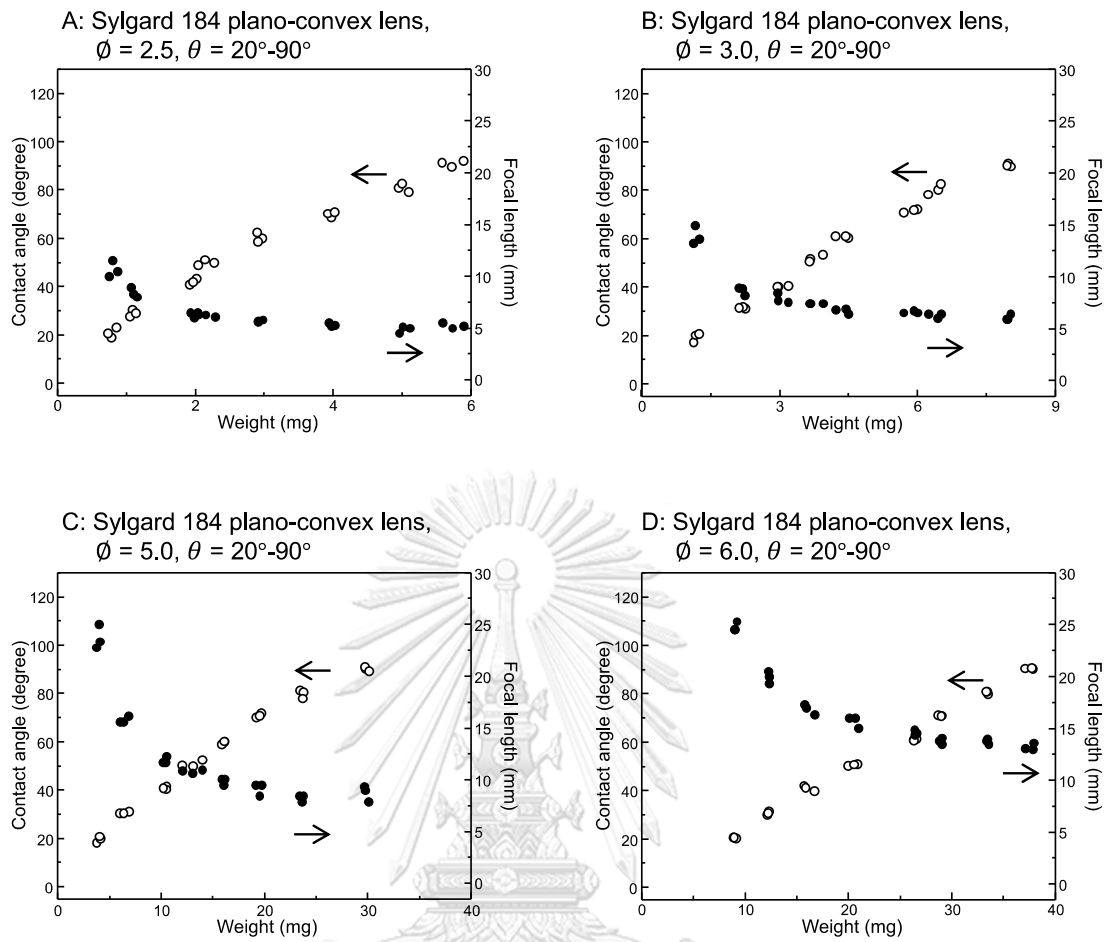
Figure 4.4 The relationship of the weight of Sylgard 184 polymer, contact angle (θ), and focal length (f) of lens fabricated on the lens substrates with various diameters at (A) 2.5, (B) 3.0, (C) 5.0, and (D) 6.0mm.

Table 4.2 The relationship of the weight of Sylgard 184 polymer, contact angle (θ), focal length (f), and the magnification (M) of lens fabricated on the lens substrates with various diameter at 2.5, 3.0, 5.0, and 6.0 mm.

Polymeric lenses	Lens diameter, $\emptyset$ (mm)	Weight (mg)	Contact angle, θ (°)	Focal length, f (mm)	Magnifi-cation, (M)
Sylgard 184 plano-convex lens	2.5	0.8 ± 0.06	20.73 ± 2.12	10.7 ± 0.76	23.4
		1.1 ± 0.04	30.05 ± 1.38	8.4 ± 0.46	29.8
		2.0 ± 0.05	41.90 ± 1.18	6.3 ± 0.29	39.5
		2.1 ± 0.22	49.94 ± 1.09	6.2 ± 0.12	40.1
		2.9 ± 0.04	60.38 ± 1.89	5.7 ± 0.10	43.9
		4.0 ± 0.05	69.88 ± 1.07	5.3 ± 0.15	46.9
		5.0 ± 0.08	80.79 ± 1.83	5.1 ± 0.32	49.7
		5.7 ± 0.16	90.98 ± 1.20	5.0 ± 0.25	50.0
	3.0	1.2 ± 0.06	19.32 ± 1.79	14.0 ± 0.89	17.9
		2.2 ± 0.07	31.39 ± 0.35	8.7 ± 0.38	28.6
		3.0 ± 0.13	40.36 ± 0.19	8.0 ± 0.47	31.4
		3.8 ± 0.17	51.93 ± 1.40	7.5 ± 0.10	33.3
		4.4 ± 0.15	60.84 ± 0.37	6.8 ± 0.26	36.8
		5.9 ± 0.16	71.55 ± 0.79	6.7 ± 0.12	37.5
		6.4 ± 0.14	80.39 ± 2.18	6.4 ± 0.23	39.3
		8.0 ± 0.04	90.39 ± 0.73	6.2 ± 0.29	40.5
	5.0	4.0 ± 0.19	19.86 ± 1.32	24.3 ± 0.89	10.3
		6.5 ± 0.42	30.73 ± 0.46	17.5 ± 0.38	14.3
		10.4 ± 0.17	41.08 ± 0.64	13.8 ± 0.47	18.1
		13.1 ± 0.97	51.04 ± 1.38	13.0 ± 0.10	19.2
		16.1 ± 0.14	59.86 ± 0.77	11.8 ± 0.26	21.1
		19.5 ± 0.26	71.11 ± 0.80	11.2 ± 0.12	22.4
		23.6 ± 0.18	79.97 ± 1.68	10.7 ± 0.23	23.4
		29.9 ± 0.21	90.30 ± 0.84	10.8 ± 0.29	23.2
	6.0	9.1 ± 0.11	20.32 ± 0.18	24.9 ± 0.46	10.1
		12.3 ± 0.07	30.52 ± 0.70	19.9 ± 0.60	12.5
		16.1 ± 0.54	40.83 ± 1.10	16.9 ± 0.51	14.8
		20.5 ± 0.44	50.42 ± 0.27	15.7 ± 0.58	16.0
		26.5 ± 0.12	60.86 ± 0.41	14.6 ± 0.26	17.1
		28.9 ± 0.19	70.78 ± 0.10	13.8 ± 0.30	18.1
		33.5 ± 0.09	80.28 ± 0.59	13.8 ± 0.25	18.2
		37.6 ± 0.44	90.25 ± 0.30	13.2 ± 0.32	18.9
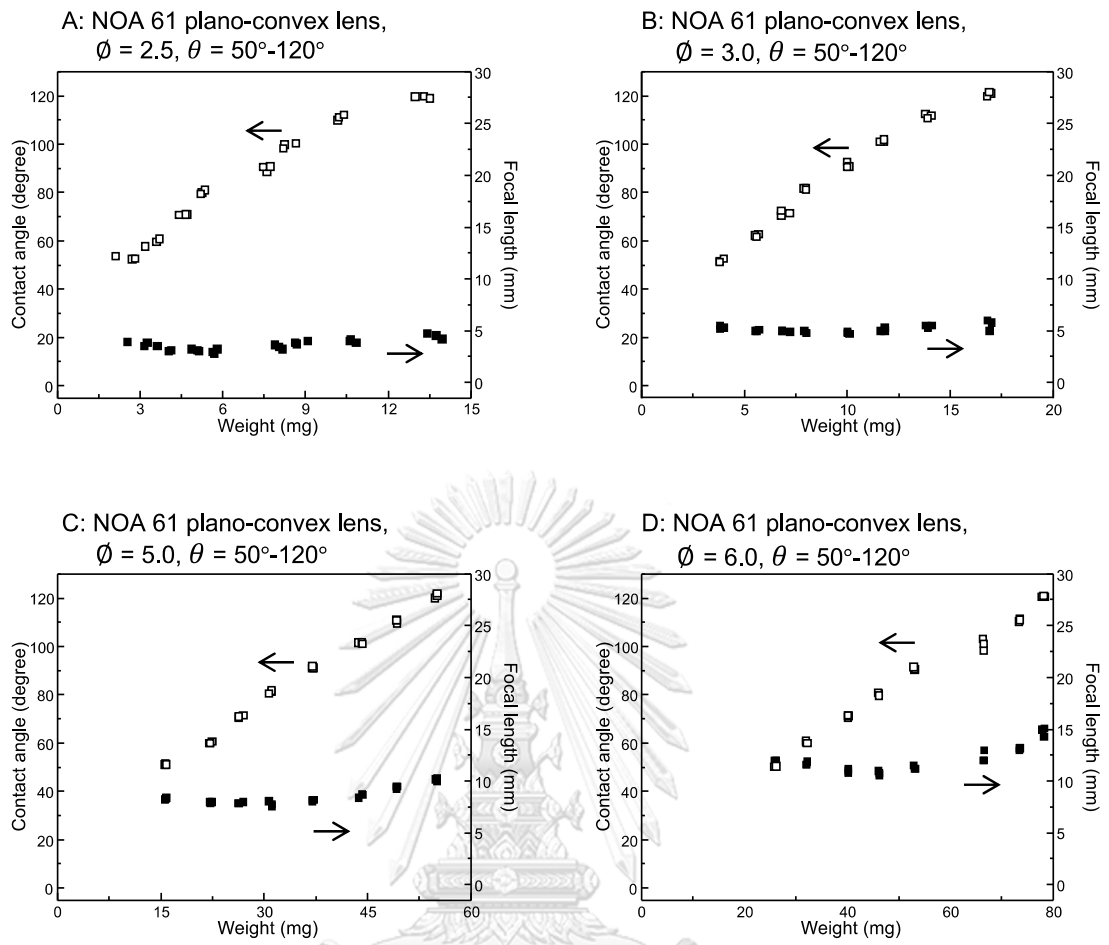
Figure 4.5 The relationship of the weight of NOA 61 polymer, contact angle (θ), and focal length of lens fabricated on the lens substrates with various diameters at (A) 2.5, (B) 3.0, (C) 5.0, and (D) 6.0mm.

Table 4.3 The relationship of the weight of NOA 61 polymer, contact angle (θ), focal length (f), and the magnification (M) of lens fabricated on the lens substrates with the various diameter at 2.5, 3.0, 5.0, and 6.0mm.

Polymeric lenses	Lens diameter, $\emptyset$ (mm)	Weight (mg)	Contact angle, θ (°)	Focal length, f (mm)	Magnifi-cation, (M)
NOA 61 plano-convex lens	2.5	2.6 ± 0.38	50.89 ± 0.65	3.7 ± 0.21	67.0
		3.5 ± 0.26	59.33 ± 1.55	3.2 ± 0.26	78.1
		4.6 ± 0.15	70.82 ± 0.12	3.1 ± 0.10	80.6
		5.3 ± 0.08	80.12 ± 0.78	3.0 ± 0.21	84.3
		7.6 ± 0.14	89.90 ± 1.25	3.4 ± 0.20	73.5
		8.4 ± 0.25	99.37 ± 1.04	3.8 ± 0.15	65.2
		10.3 ± 0.12	111.07 ± 1.17	4.0 ± 0.15	63.0
		13.3 ± 0.27	119.43 ± 0.46	4.5 ± 0.25	56.0
	3.0	3.9 ± 0.12	51.09 ± 0.70	5.3 ± 0.15	46.9
		5.6 ± 0.10	61.45 ± 0.46	5.0 ± 0.06	49.7
		6.9 ± 0.23	70.72 ± 1.06	5.0 ± 0.06	50.3
		8.0 ± 0.06	80.85 ± 0.36	4.9 ± 0.12	51.4
		10.0 ± 0.06	90.58 ± 1.11	4.8 ± 0.10	52.1
		11.7 ± 0.12	100.55 ± 0.55	5.1 ± 0.17	49.0
		13.9 ± 0.15	110.90 ± 0.93	5.4 ± 0.12	46.0
		16.9 ± 0.10	120.04 ± 0.95	5.6 ± 0.53	44.6
	5.0	15.7 ± 0.10	51.20 ± 0.32	8.3 ± 0.10	30.1
		22.3 ± 0.21	60.15 ± 0.32	8.0 ± 0.06	31.4
		26.4 ± 0.40	70.90 ± 0.41	7.9 ± 0.06	31.5
		31.0 ± 0.23	81.06 ± 0.60	7.8 ± 0.25	31.9
		37.1 ± 0.12	91.18 ± 0.48	8.2 ± 0.06	30.6
		44.1 ± 0.32	101.25 ± 0.32	8.6 ± 0.21	29.0
		49.2 ± 0.06	110.36 ± 0.75	9.4 ± 0.12	26.5
		55.0 ± 0.17	120.95 ± 0.96	10.2 ± 0.15	24.6
	6.0	26.1 ± 0.15	50.43 ± 0.45	11.9 ± 0.12	20.9
		32.1 ± 0.12	60.28 ± 0.54	11.7 ± 0.17	21.4
		40.1 ± 0.06	71.03 ± 0.46	11.0 ± 0.20	22.7
		46.1 ± 0.12	80.26 ± 0.53	10.8 ± 0.20	23.1
		53.1 ± 0.15	90.75 ± 0.58	11.3 ± 0.17	22.1
		66.5 ± 0.06	100.67 ± 0.47	12.3 ± 0.58	20.3
		73.5 ± 0.10	110.85 ± 057	13.1 ± 0.12	19.0
		78.1 ± 0.21	120.67 ± 0.23	14.8 ± 0.44	16.9

4.1.3 Effect of gravitational force

The interplay between the surface tension and gravitational force affects the formation of droplets [67, 68]. The increase in the gravitational effect causes the droplet deformation. However, the gravitational force is negligible if the droplet placed on a horizontal surface is small enough [69]. Since the geometry of the polymer droplet affects the lens parameter, we investigate the effect of gravity on the droplet formation. The gravitational effects on the lens envelope were compared with and without gravity. For the lens formation without gravitational effect, we simulated the lens envelope of all size of the fabricated lenses (2.5-6.0 mm diameter of the lens substrates) using ImageJ program public domain license with Java-based image processing developed by National Institutes of Health, USA, along with a drop snake plug-in (based on ImageJ software).

Figure 4.6-4.10 and Table 4.4-4.8 are envelope profiles and lens parameters, respectively, showing the relationship between the lens envelope and θ. The results show that the envelop height of fabricated lenses gradually decreases as the contact angle increased. For the small lens substrate (2.5-4.0 mm), the significant decrease of lens height, together with the increasing radius of lens curvature (R), was observed at the value of θ is more than 70°. For the big lens substrates (5.0-6.0 mm), the deformation when the value of θ is more than 50°.

As mention above, the formation of the droplet placed in horizontal is the interplay of surface tension and gravity. The surface tension pulls back the liquid from spreading and form the curvature to reduce the surface energy. Meanwhile, the gravity pushes down, resulting in the deformation of the droplets. In the case of the small droplet, the surface tension overwhelms the gravity effect due to the small

weight. This causes the perfect hemispherical shape of droplets. However, when the weight of droplet increases, the gravitational dictates the deformation of the droplets.

Figure 4.6 Envelop of Sylgard 184 (red line), NOA 61 (blue line), and simulated hemispherical (dash line) plano-convex lenses fabricated on the 2.5 mm lens substrates with contact angle (θ) of (A) 20 degrees, (B) 30 degrees, (C) 40 degrees, (D) 50 degrees, (E) 60 degrees, (F) 70 degrees, (G) 80 degrees, (H) 90 degrees, (I) 100 degrees, (J) 110 degrees, and (K) 120 degrees.

Table 4.4 Comparison of lens height (H) and radius of lens curvature (R) between the simulated and fabricated plano-convex lens on 2.5 mm lens substrates.

Polymeric lens	Lens diameter, Ø (mm)	Contact angle, θ (°)	Height of lenses, H (mm)		Radius of lens curvature, R (mm)	
			Theory	Experiment	Theory	Experiment
Sylgard 184 plano-convex lens	2.5	20	0.22	0.20	3.65	3.92
		30	0.33	0.32	2.50	2.63
		40	0.45	0.50	1.94	1.82
		50	0.58	0.52	1.63	1.75
		60	0.72	0.69	1.44	1.48
		70	0.88	0.87	1.33	1.33
		80	1.05	0.96	1.27	1.29
		90	1.25	1.19	1.25	1.25
NOA 61 plano-convex lens	2.5	50	0.58	0.59	1.63	1.62
		60	0.72	0.65	1.44	1.52
		70	0.88	0.85	1.33	1.34
		80	1.05	0.98	1.27	1.29
		90	1.25	1.26	1.25	1.25
		100	1.49	1.38	1.27	1.26
		110	1.79	1.49	1.33	1.27
		120	2.17	1.61	1.44	1.29

จุฬาลงกรณ์มหาวิทยาลัย

CHULALONGKORN UNIVERSITY

Figure 4.7 Envelop of Sylgard 184 (red line), NOA 61 (blue line), and simulated hemispherical (dash line) plano-convex lenses fabricated on the 3.0 mm lens substrates with contact angle (θ) of (A) 20 degrees, (B) 30 degrees, (C) 40 degrees, (D) 50 degrees, (E) 60 degrees, (F) 70 degrees, (G) 80 degrees, (H) 90 degrees, (I) 100 degrees, (J) 110 degrees, and (K) 120 degrees.

Table 4.5 Comparison of lens height (H) and radius of lens curvature (R) between the simulated and fabricated plano-convex lens on 3.0 mm lens substrates.

Polymeric lens	Lens diameter, $\emptyset$ (mm)	Contact angle, θ (°)	Height of lenses, H (mm)		Radius of lens curvature, R (mm)	
			Theory	Experiment	Theory	Experiment
Sylgard 184 plano-convex lens	3.0	20	0.26	0.27	4.39	4.32
		30	0.40	0.45	3.00	2.71
		40	0.55	0.59	2.33	2.20
		50	0.70	0.71	1.96	1.94
		60	0.87	0.92	1.73	1.69
		70	1.05	1.05	1.60	1.60
		80	1.26	1.13	1.52	1.56
		90	1.50	1.23	1.50	1.53
NOA 61 plano-convex lens	3.0	50	0.70	0.74	1.96	1.89
		60	0.87	0.89	1.73	1.71
		70	1.05	1.07	1.60	1.59
		80	1.26	1.20	1.52	1.54
		90	1.50	1.40	1.50	1.50
		100	1.79	1.49	1.52	1.50
		110	2.14	1.67	1.60	1.51
		120	2.60	1.83	1.73	1.53

จุฬาลงกรณ์มหาวิทยาลัย

CHULALONGKORN UNIVERSITY

Figure 4.8 Envelop of Sylgard 184 (red line), NOA 61 (blue line), and simulated hemispherical (dash line) plano-convex lenses fabricated on the 4.0 mm lens substrates with contact angle (θ) of (A) 20 degrees, (B) 30 degrees, (C) 40 degrees, (D) 50 degrees, (E) 60 degrees, (F) 70 degrees, (G) 80 degrees, (H) 90 degrees, (I) 100 degrees, (J) 110 degrees, and (K) 120 degrees.

Table 4.6 Comparison of lens height (H) and radius of lens curvature (R) between the simulated and fabricated plano-convex lens on 4.0 mm lens substrates.

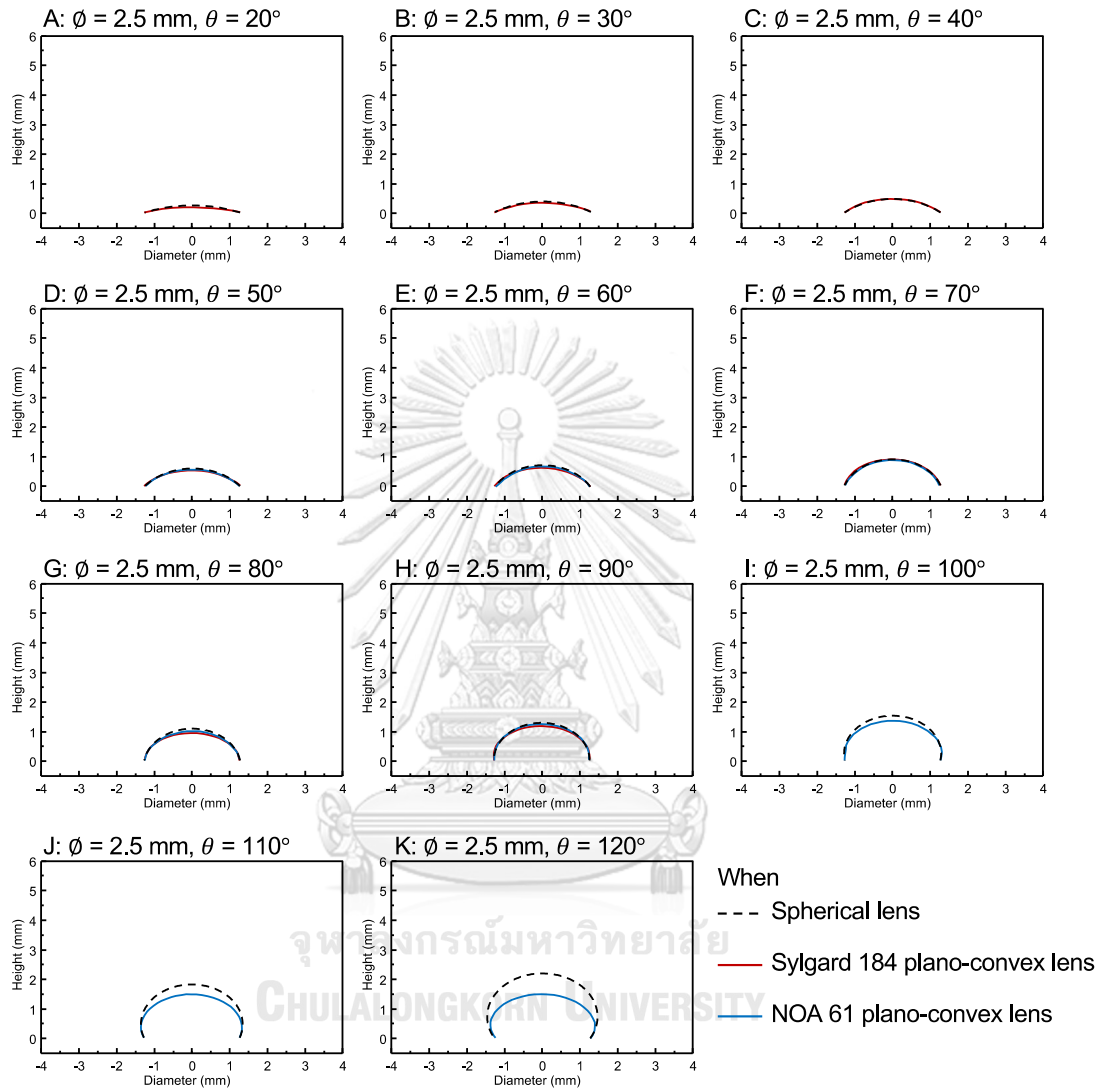| Polymeric lens	Lens diameter, $\emptyset$ (mm)	Contact angle, θ (°)	Height of lenses, H (mm)		Radius of lens curvature, R (mm)	
			Theory	Experiment	Theory	Experiment
Sylgard 184 plano-convex lens	4.0	20	0.35	0.36	5.85	5.81
		30	0.54	0.48	4.00	4.40
		40	0.73	0.61	3.11	3.60
		50	0.93	0.86	2.61	2.76
		60	1.15	1.07	2.31	2.40
		70	1.40	1.14	2.13	2.32
		80	1.68	1.36	2.03	2.15
		90	2.00	1.58	2.00	2.06
NOA 61 plano-convex lens	4.0	50	0.93	0.82	2.61	2.84
		60	1.15	1.04	2.31	2.44
		70	1.40	1.27	2.13	2.21
		80	1.68	1.45	2.03	2.10
		90	2.00	1.62	2.00	2.04
		100	2.38	1.83	2.03	2.01
		110	2.86	2.01	2.13	2.00
		120	3.46	2.13	2.31	2.00

จุฬาลงกรณ์มหาวิทยาลัย

CHULALONGKORN UNIVERSITY
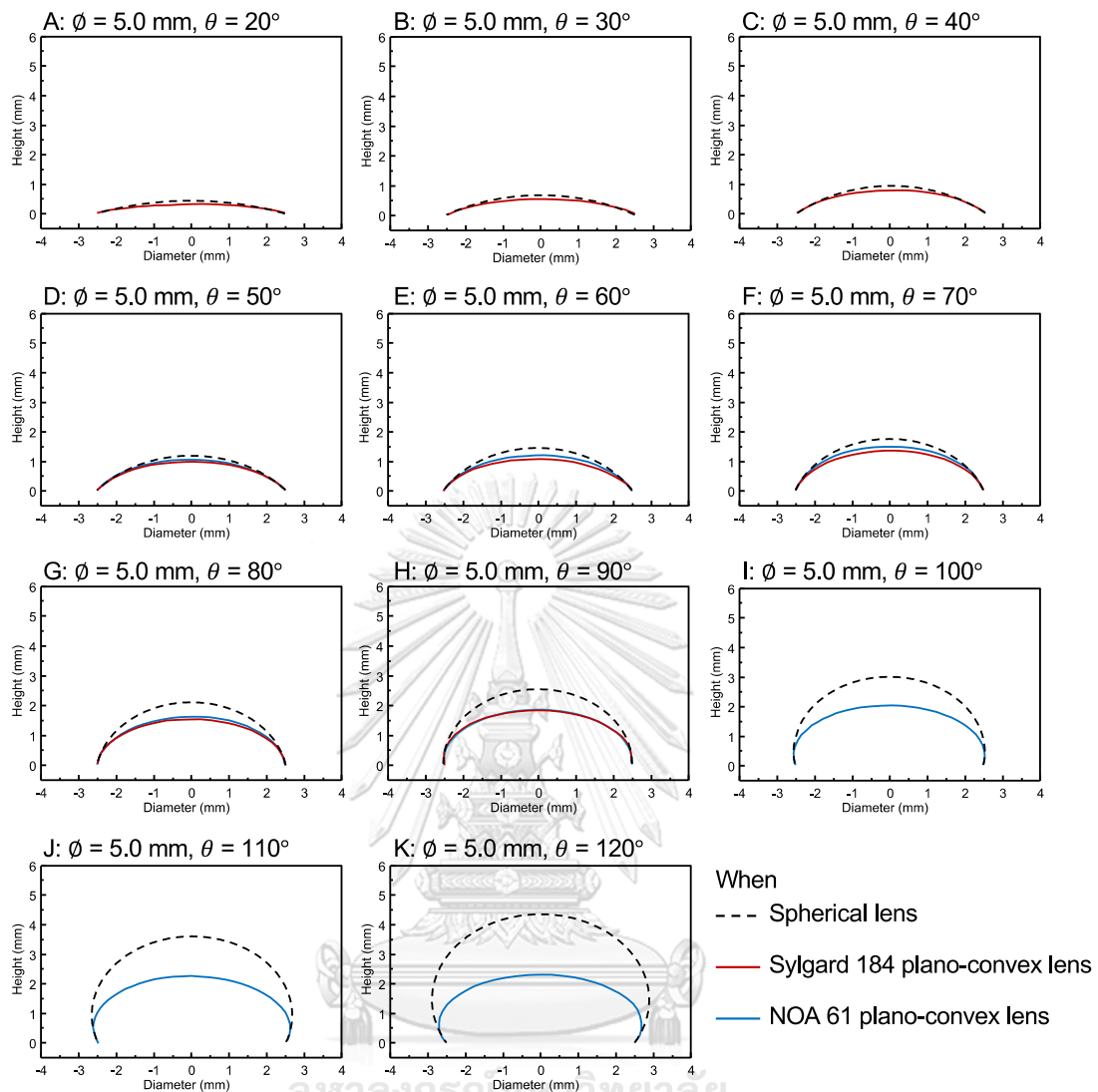
Figure 4.9 Envelop of Sylgard 184 (red line), NOA 61 (blue line), and simulated hemispherical (dash line) plano-convex lenses fabricated on the 5.0 mm lens substrates with contact angle (θ) of (A) 20 degrees, (B) 30 degrees, (C) 40 degrees, (D) 50 degrees, (E) 60 degrees, (F) 70 degrees, (G) 80 degrees, (H) 90 degrees, (I) 100 degrees, (J) 110 degrees, and (K) 120 degrees.

Table 4.7 Comparison of lens height (H) and radius of lens curvature (R) between the simulated and fabricated plano-convex lens on 5.0 mm lens substrates.

Polymeric lens	Lens diameter, Ø (mm)	Contact angle, θ (°)	Height of lenses, H (mm)		Radius of lens curvature, R (mm)	
			Theory	Experiment	Theory	Experiment
Sylgard 184 plano-convex lens	5.0	20	0.44	0.34	7.31	9.48
		30	0.67	0.55	5.00	5.94
		40	0.91	0.80	3.89	4.30
		50	1.17	0.97	3.26	3.71
		60	1.44	1.07	2.89	3.45
		70	1.75	1.36	2.66	2.98
		80	2.10	1.53	2.54	2.81
		90	2.50	1.83	2.50	2.62
NOA 61 plano-convex lens	5.0	50	1.17	1.07	3.26	3.46
		60	1.44	1.32	2.89	3.02
		70	1.75	1.48	2.66	2.85
		80	2.10	1.65	2.54	2.72
		90	2.50	1.88	2.50	2.60
		100	2.98	2.01	2.54	2.56
		110	3.57	2.23	2.66	2.52
		120	4.33	2.29	2.89	2.51

จุฬาลงกรณ์มหาวิทยาลัย
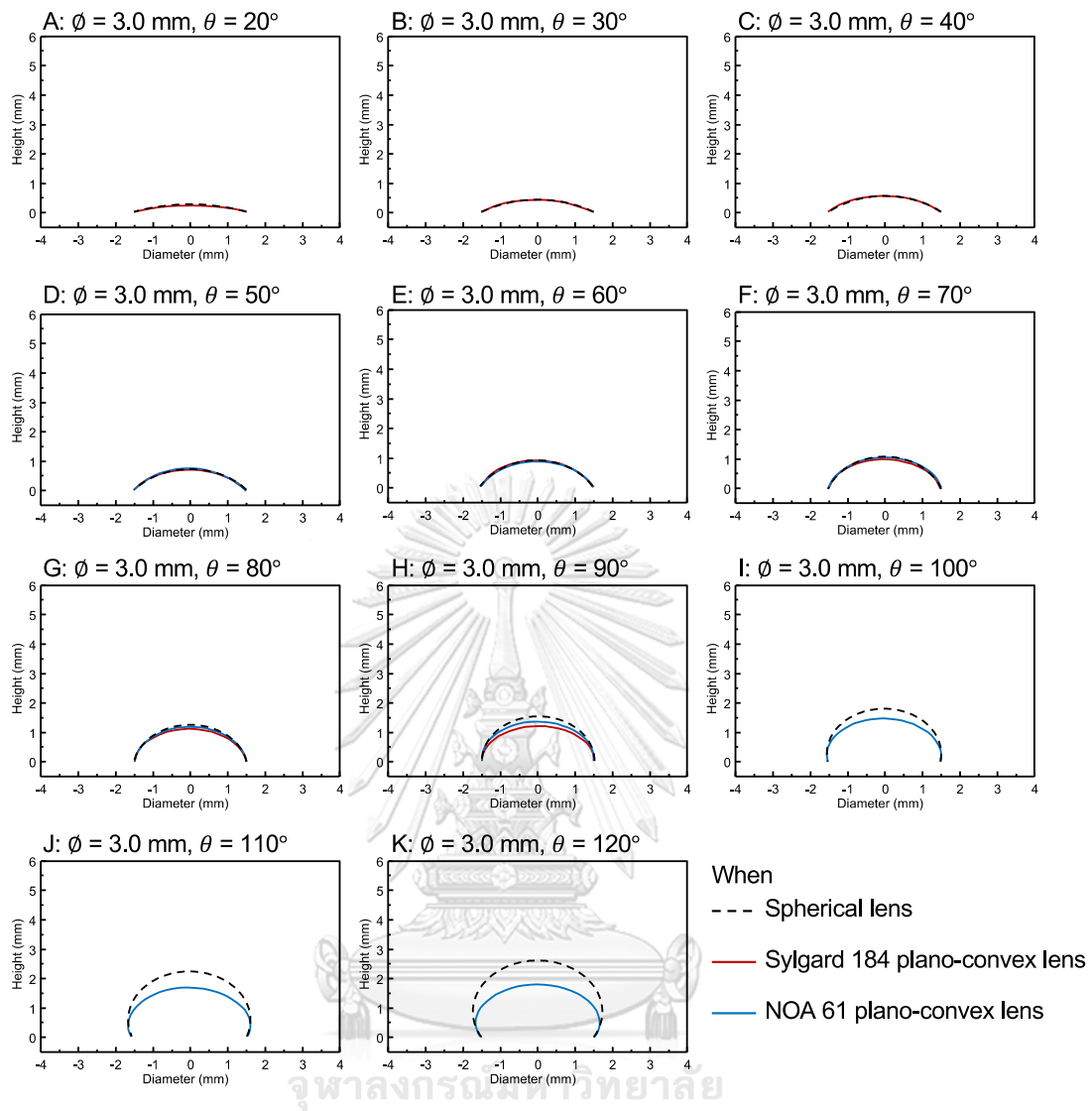
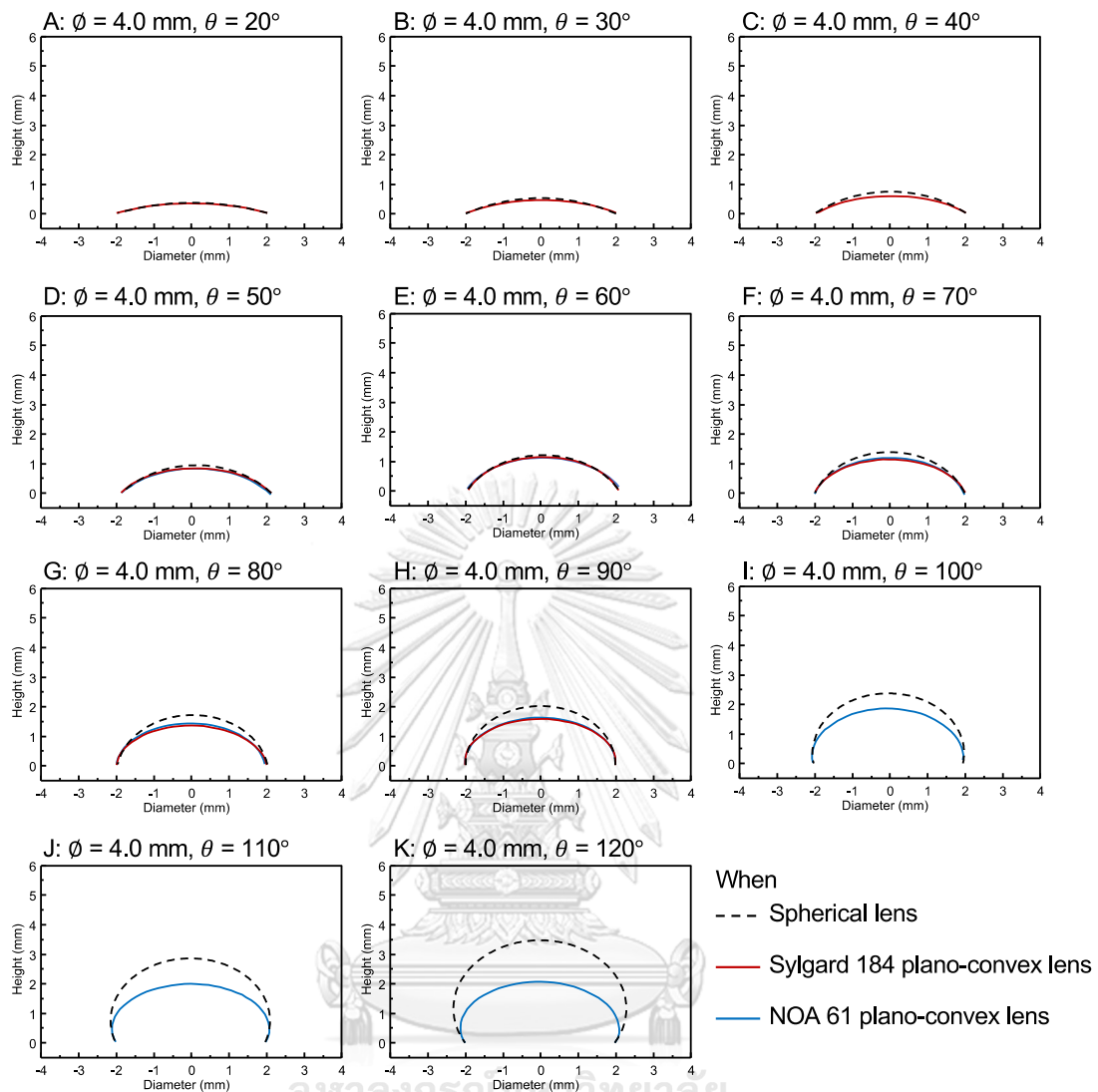CHULALONGKORN UNIVERSITY
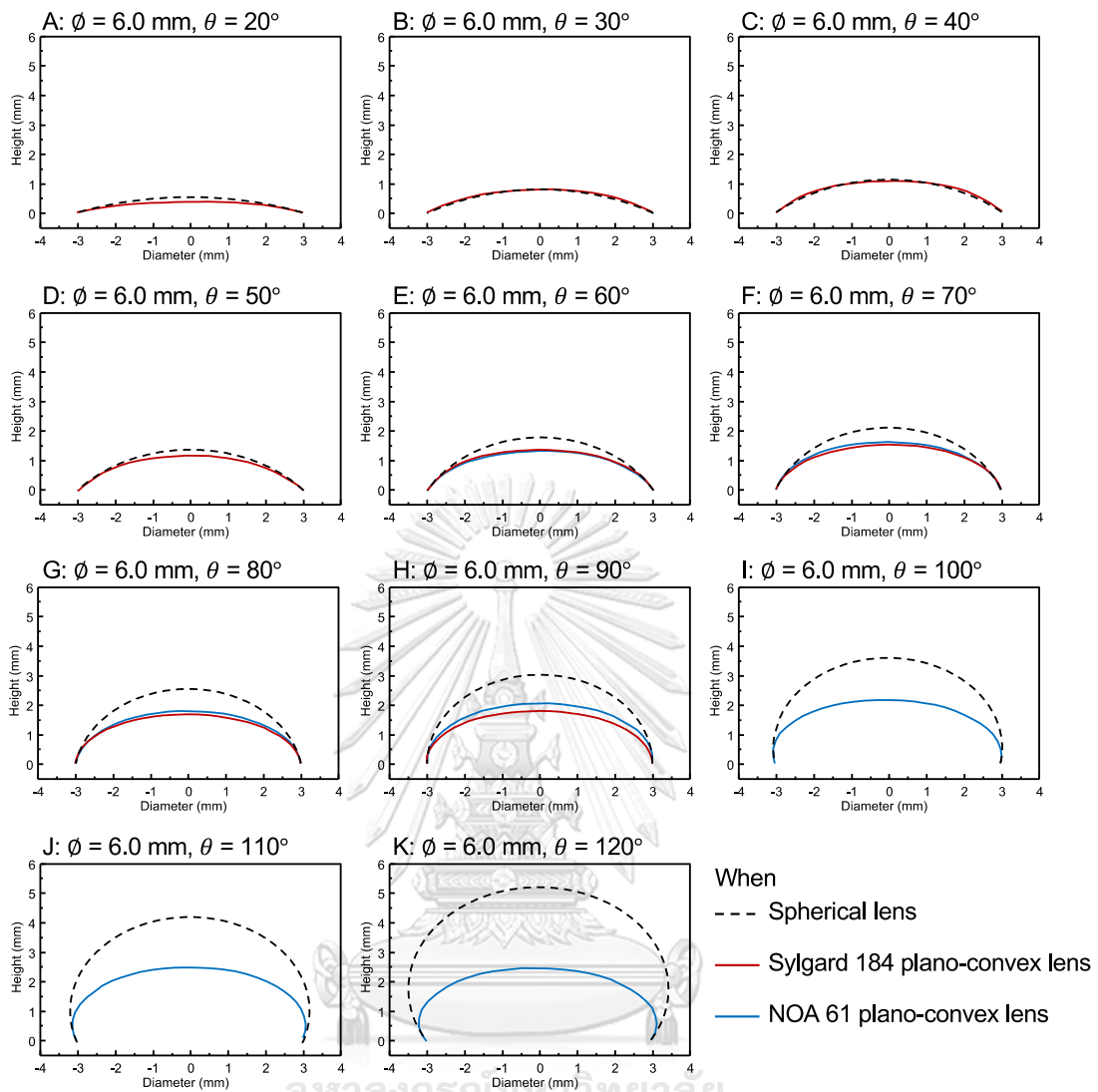
Figure 4.10 Envelop of Sylgard 184 (red line), NOA 61 (blue line), and simulated hemispherical (dash line) plano-convex lenses fabricated on the 6.0 mm lens substrates with contact angle (θ) of (A) 20 degrees, (B) 30 degrees, (C) 40 degrees, (D) 50 degrees, (E) 60 degrees, (F) 70 degrees, (G) 80 degrees, (H) 90 degrees, (I) 100 degrees, (J) 110 degrees, and (K) 120 degrees.

Table 4.8 Comparison of lens height (*H*) and radius of lens curvature (*R*) between the

simulated and fabricated plano-convex lens on 6.0 mm lens substrates.

Polymeric lens	Lens diameter, Ø (mm)	Contact angle, θ (°)	Height of lenses, *H* (mm)		Radius of lens curvature, *R* (mm)	
			Theory	Experiment	Theory	Experiment
Sylgard 184 plano-convex lens	6.0	20	0.53	0.42	8.77	11.03
		30	0.80	0.82	6.00	5.90
		40	1.09	1.09	4.67	4.68
		50	1.40	1.21	3.92	4.32
		60	1.73	1.39	3.46	3.93
		70	2.10	1.47	3.19	3.80
		80	2.52	1.68	3.05	3.52
		90	3.00	1.78	3.00	3.42
NOA 61 plano-convex lens	6.0	50	1.40	1.25	3.92	4.21
		60	1.73	1.33	3.46	4.05
		70	2.10	1.60	3.19	3.61
		80	2.52	1.81	3.05	3.39
		90	3.00	2.04	3.00	3.23
		100	3.58	2.17	3.05	3.16
		110	4.28	2.41	3.19	3.07
		120	5.20	2.44	3.46	3.06

จุฬาลงกรณ์มหาวิทยาลัย

CHULALONGKORN UNIVERSITY

The lens geometry affects the focal length of the fabricated lens. In principle, the plano-convex lens with a 90° of contact angle is a perfect hemispherical shape. The radius of lens curvature (R) and the radius of lens (r, r = $\emptyset/2$, when $\emptyset$ is lens diameter) are equal. Considering, we can be calculated the focal length from Lens maker's equation (equation 2.2) for the theoretical focal length. However, in this experiment, the deformation of lens shape caused by gravity is observed. The deformation can alter the theoretical focal length described by Lens maker's equation.

We measured the focal length of the lenses with 90° of contact angle formed on the various sizes of the lenses. Then, the measured focal length was compared to the calculation values. Figure 4.11 shows the relationships between the focal length and lens diameter. For the Sylgard 184 plano-convex lens, the measured focal length values are higher than the calculation value for all diameter. Meanwhile, the measured focal length of NOA 61 plano-convex lens with a diameter of 2.5 mm matches with the calculation value. However, when the lens diameter is more than 2.5 mm, the measured focal length is higher than the calculation value. According to the Lens maker's equation, the radius of lens curvature is one of the parameters that use for calculations. The gravitational force dictates the deformation of the lens resulting in the increase of radius of lens curvature from the ideal plano-convex lens. This results in the longer focal length in the fabricated lens compared to the calculated values. However, for the NOA 61 plano-convex lens with diameter of 2.5 mm, the gravitational force does not significantly affect on the radius of lens curvature. Thus, the measured and the calculated focal length is the same.
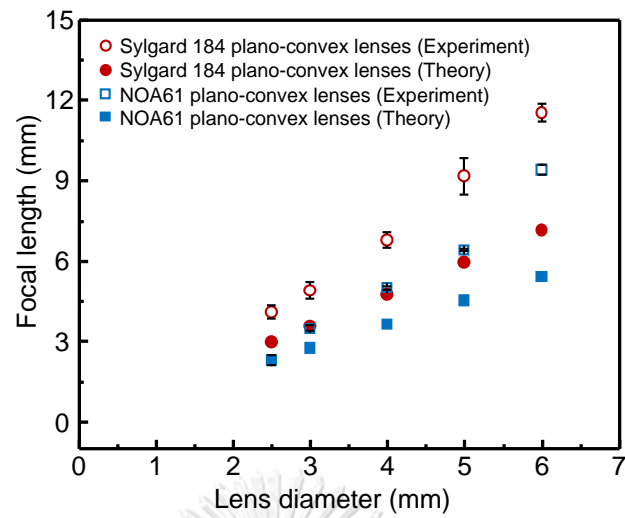
Figure 4.11 Comparison of the change of lens diameter with the focal length between (open symbol) experimental measurement and theoretical calculation. Note: All of the lenses have a contact angle of 90°.

4.1.4 The performance of the fabricated lenses

The resolution is the most common parameter used to evaluate the performance of the optical system. The resolution is widely presented in terms of line-pair per millimeter (lp/mm), where a bar (white) and a space (black) equal one line-pairs. A high-resolution image is a great detail and clear, whereas a low-resolution image is fine default detail and blurry. High performance of lens has high resolution, which can resolvable more the number of line pairs in 1 millimeter. The resolution can determine by considering of the group number and element number following table 4.10 [70].

The performance of the lens was evaluated through the image resolution and contrast, which inspected from the 1951 USAF patterns. The contrast is the measurement of the ability to separate the light and dark areas of an image. It is normally indicated in terms of percentage as follows:

$$\% \text{ contrast} = \left(\frac{I_{max} - I_{min}}{I_{max} + I_{min}} \right) \times 100 \tag{4.1}$$

Where I_{min} and I_{max} are the minimum and maximum intensity, respectively.

The darkest blacks produced high intensity, whereas the brightest whites also produced low intensity. The highest contrast is the darkest blacks and the brightest whites in the image without shades of gray in between, which is the 100 percent contrast. Oppositely, the lowest contrast is provided 0 percent contrast. When the black and the white begin to blur and the shade of gray present, the percent contrast in the image reduces.

Table 4.9 Number of lp/mm in the 1951 USAF patterns [70]

Element number	Group number					
	2	3	4	5	6	7
1	4.00	8.00	16.00	32.00	64.00	128.00
2	4.49	8.98	17.96	35.90	71.80	143.70
3	5.04	10.08	20.16	40.30	80.60	161.30
4	5.66	11.31	22.63	45.30	90.50	181.00
5	6.35	12.70	25.40	50.80	101.60	203.20
6	7.13	14.25	28.51	57.00	114.00	228.10

We investigate the performance of the fabricated lenses using the combined resolution/distortion test target, called 1951 USAF (R1S1L1N, Negative Test Targets, Thorlabs Inc.) The high-performance optical microscope (Carl Zeiss: Axio Scope.A1) was the benchmark against the smartphone microscope, which uses 50x Sylgard 184 and 50x NOA 61 as the attachments. As shown in Figure 4.12, the fabricated lens can observe the combined resolution/distortion test target at group 4 element 1 and group 4 element 2. For group 4 element 1, the microscope and the fabricated lens can provide a resolution of 16.00 lp/mm with a line width of 31.25 µm (Table 4.9). However, the high-performance microscope provides exceptional percent contract of above 90% for horizontal and vertical lines (Table 4.10, Figure 4.12). Meanwhile, the Sylgard 184 and NOA 61 provide much lower in percent contract for both horizontal and vertical lines. For Sylgard 184 lens, the percent contract of horizontal and vertical lines are 13.2 and 20.7%, respectively. The NOA 61 lens provides the percent contract of horizontal and vertical lines are 25.6 and 19.6%, respectively (Table 4.10,

Figure 4.12). Besides, the appropriate value of percent contrast is more than 20 percent [71-74]. For the fabricated lenses, the percent contract is acceptable.

For group 4 element 2 (the resolution of 17.96 lp/mm and the line width of 27.84), the high-performance microscope still has an excellent percent contract of 91.9 and 89.3 for horizontal and vertical lines, respectively (Table 4.10, Figure 4.12). The Sylgard 184 plano-convex lens provides an unacceptable performance with the percent contract of 17.9 and 13.9% horizontal and vertical, respectively. The NOA 61 plano-convex lens still has the acceptable performance with the percent contract of horizontal and vertical lines are 17.8 and 21.8%, respectively (Table 4.10, Figure 4.12).

Table 4.10 Intensity of group 4 element 1and element 2 in 1951 USAF patterns

Image with	Optical microscope (Axio Scope.A1)		Sylgard 184 plano-convex lens		NOA 61 plano-convex lens	
Group 4 Element 1						
Resolution (μm)	31.25(III)	31.25($\equiv$)	31.25(III)	31.25($\equiv$)	31.25(III)	31.25($\equiv$)
I_{max}	213	215	191	179	181	181
I_{min}	9	8	126	138	122	107
% Contrast	91.9	92.8	20.7	13.2	19.6	25.6
Group 4 Element 2						
Resolution (μm)	27.84(III)	27.84($\equiv$)	27.84(III)	27.84($\equiv$)	27.84(III)	27.84($\equiv$)
I_{max}	213	213	180	192	187	185
I_{min}	12	9	136	134	120	129
% Contrast	89.3	91.9	13.9	17.9	21.8	17.8
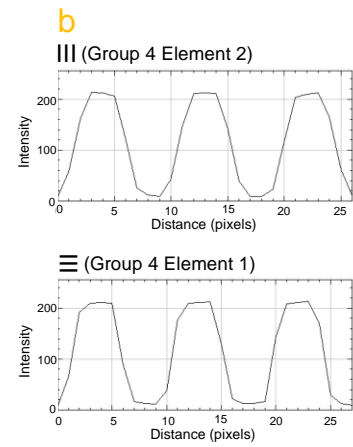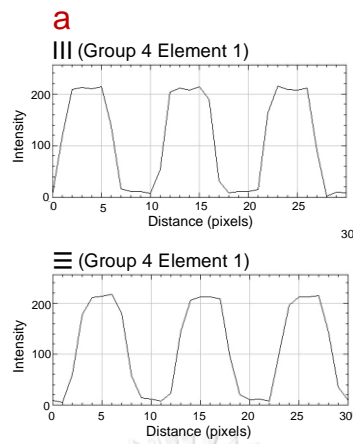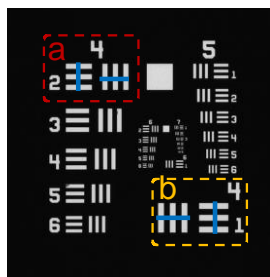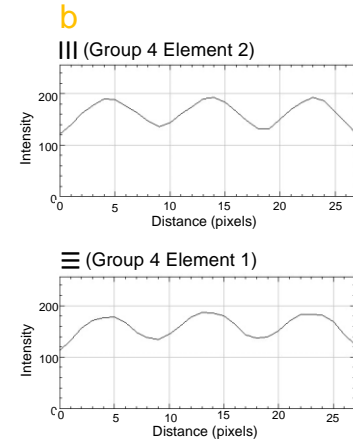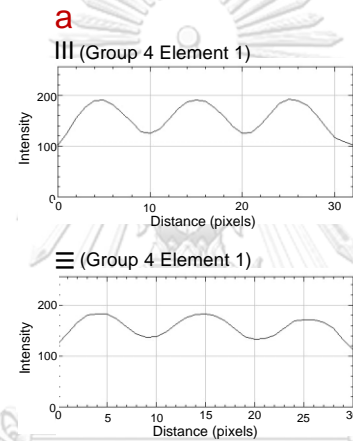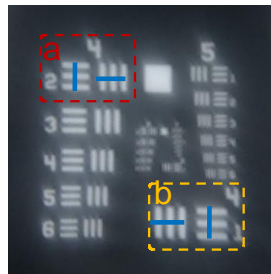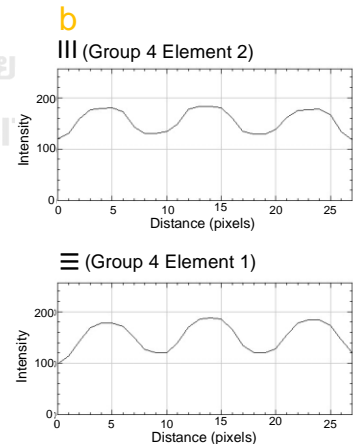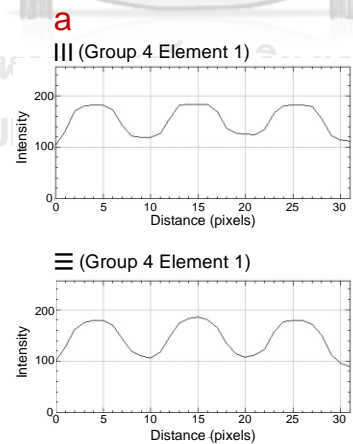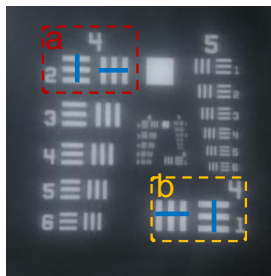
Figure 4.12 Image of 1951 USAF resolution target taken by (A) optical microscope, (B) 50x Sylgard 184 plano-convex lens, and (C) 50x NOA 61 plano-convex lens. The resolvable features of (a) group 4 element 1 and (b) group 4 element 2. The blue lines in (A), (B), and (C) are the analyzing the intensity line.

4.2 Smartphone microscopy application

One of the promising application of the polymeric plano-convex lens is to utilize it as an external attachment for converting a conventional smartphone to a portable smartphone microscope. The handy-size of the smartphone with a superb image sensor allows the smartphone microscope to be an excellent micro imaging device for analysis both in the field and in the laboratory. We demonstrate the performance of the lens for smartphone microscope application by taking the pixel images of the iPhone 7 display compared with the laboratory mi microscope. Besides, the smartphone displays are made up of tiny individual picture elements, called pixels. Each pixel is consisting of sub-pixels which represent in either three color components, known as, RGB color model (Red, Green, and Blue) or four color components, known as CMYK color model (Cyan, Magenta, Yellow, and blacK). The feature pixels in each smartphone displays are difference, such as LCD, and OLED/AMOLED. The iPhone 7 display is the LCD. The LCD is the traditional feature display. Its sub-pixel is RGB color model, which a standard arrangement. Apple's reported that the resolution and the pixel density of the iPhone 7 display are 750 x 1334 px and 326 ppi (pixels per inch), respectively [75]. From the calculation, the one unit pixel of the iPhone 7 smartphone display has a length of 78 μm [76].

Figure 4.13 shows the macrographs of the pixels on iPhone 7 displays taken form laboratory microscope and the smartphone microscopy. The images were captured with the same magnification at 50x, 100x, and 200x. The image magnification of the microscope is the true optical magnification, while the image magnification of smartphone microscope is the combination of optical and digital magnification. The results show that the width and the length of pixels measured from

both microscope and smartphone microscope are 62 and 75 µm, respectively. Although the actual size of the pixel did not equal the reported value, the size of pixels measured from smartphone microscope is the same as the laboratory microscope. For the quality of the images, the laboratory microscopy shows a much better image quality in both color and contrast. In a smartphone microscope, the color distortion, pale color, and blurry appeared. At high magnification (100x and 200x), the sharpness of the image dramatically reduced due to the increase of noise on the picture, Figure B2, B3, C2, and C3. Although the quality of the image of the smartphone microscope cannot beat those image quality from the lab microscope, however the lower price of the plano-convex lens still the major advantage that enables the exploration of microscopy in a penny.

We further demonstrate the usage of polymeric plano-convex lenses in the real application. We utilized the smartphone microscope attached with Sylgard 184 plano-convex lens and 20x NOA 61 plano-convex lenses to inspect the PCB and the nozzle of 3D printer. As shown in Figure 4.14, we can observe details on small objects, such as the number on PCB and the fault point on the nozzle.
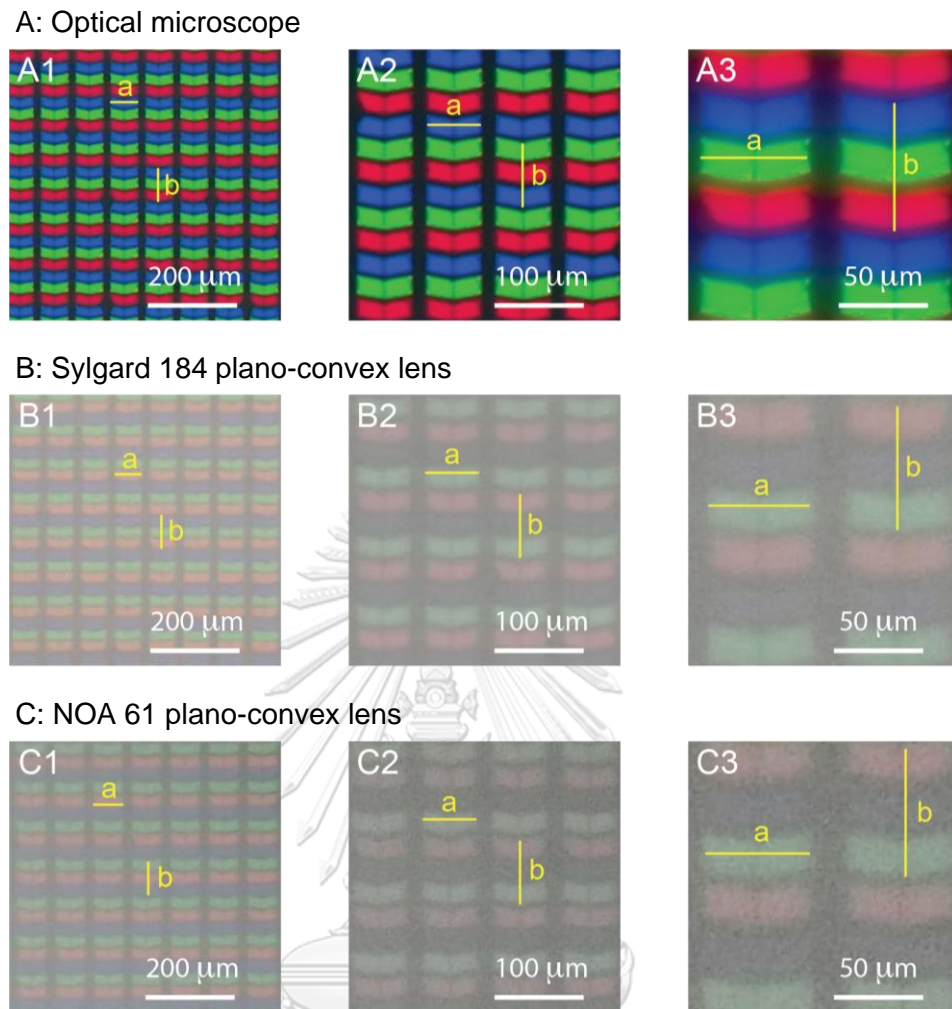
Figure 4.13 Digital micrographs showing the pixels on iPhone 7 displays taken by (A) high-performance optical microscope (Carl Zeiss: Axio Scope.A1) and the smartphone model Huawei 20 pro attached with (B) 50x Sylgard 184 and (C) 50x NOA 61 plano-convex lens. The magnification of the digital micrographs are (1) 50x, (2) 100x, and (3) 200x, respectively. For the micrographs taken from the high-performance optical microscope, all magnification is the true optical magnification, while those taken from the smartphone are the combination between 50x optical magnification and digital magnification (50x = 50x optical magnification, 100x = 50x optical and 2x digital magnification, 200x = 50x optical and 4x digital magnification). The bars a and b indicate the width and length of a pixel, respectively.
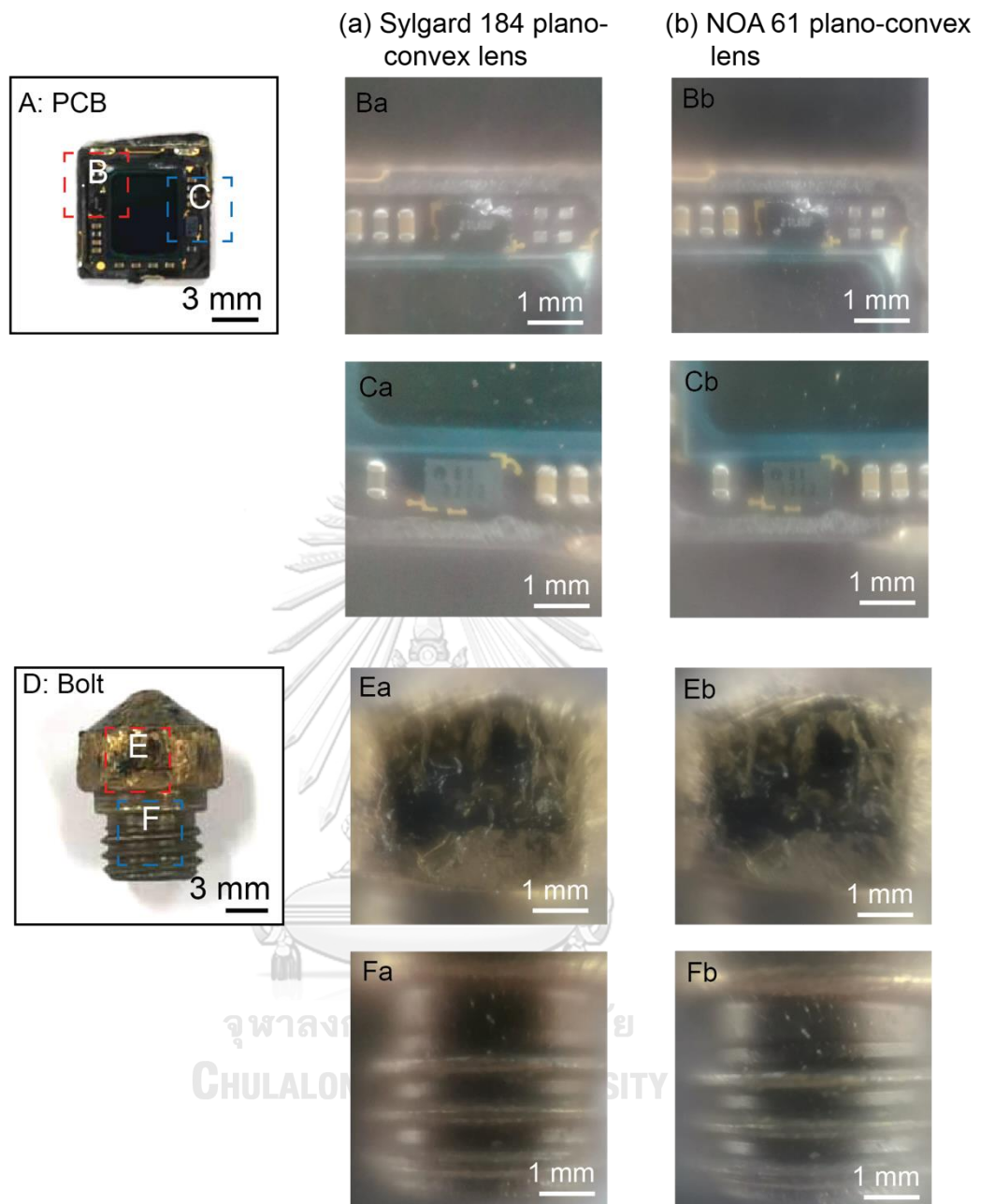
Figure 4.14 (A) A digital photograph of a PCB. (B) and (C) Digital macrographs taken from the PCB. (D) A Digital photograph of a nozzle head of a 3-D printer. (E) and (F) Digital macrographs took from the nozzle head. The macrographs taken by a smartphone model Huawei P20Pro attached with (a) 20x Sylgard 184 and (b) 20x NOA 61 plano-convex lenses.

4.3 SPR sensor chip

In the conventional SPR application, the optical prism is used to couple the incident light to the metal surface. Generally, high refractive materials, such as BK-7, SF5, SF10 and SF11, which has the refractive index in range of 1.51 to 1.72., are preferred [61, 77-80]. The NOA 61 plano-convex lens has a refractive index of 1.56 that suitable for utilization as the SPR prism. Thus, we interested in the modification of the NOA 61 plano-convex lens to be used as the SPR prism. The use of the NOA 61 plano-convex lens in the miniature SPR sensor chip provides a small device that reduces the cost, compared to the high-quality prism.

To demonstrate the potential of the NOA 61 plano-convex lens as the SPR sensor chip, we modified the NOA 61 plano-convex lens by forming of 3 nm Cr and 47 nm Au film on the planar site of the lens, producing the SPR sensor based on Krestchmann configuration. Then, the chip was mounted in a 3D-printed flow cell by using liquid NOA 61 as a glue (Figure 3.9). The 3D-printed flow cell uses only 280 µL of liquid to fill up. We used the wavelength-modulated SPR characterization for demonstrate the potential of the miniature SRP sensor chip. Figure 4.15 shows the SPR reflectivity curves obtained from different incident light angle at 45°, 50°, 55°, 60°, and 65°, which characterized in air (n = 1.00). The increase of the incident angle causes blue shift of the SPR dips. We demonstrate the use of the SPR to monitor the change of the refractive index of dielectric media at 63°. We inspected the change of the SPR dips as the refractive index of dielectric media change from water (n = 1.33) to 20% w/w Ethylene glycol (n = 1.35) [81]. As shown in Figure 4.16, the redshift of the resonance wavelength from 565 to 582 nm. This indicates that the miniature SPR

sensor chips sense to the change of refractive index of dielectric media and can be used in the real SPR application to as biosensor and so on.
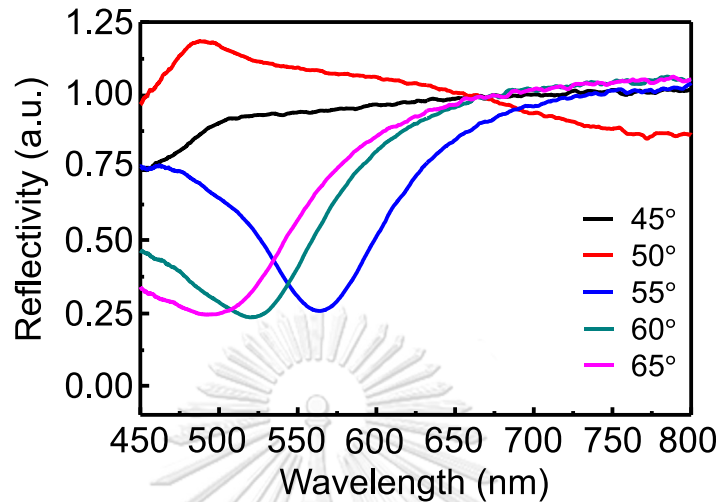
Figure 4.15 SPR reflectivity curves of air (n = 1.00) from the use of the miniature SPR sensor chip with diameter 6.0 mm.
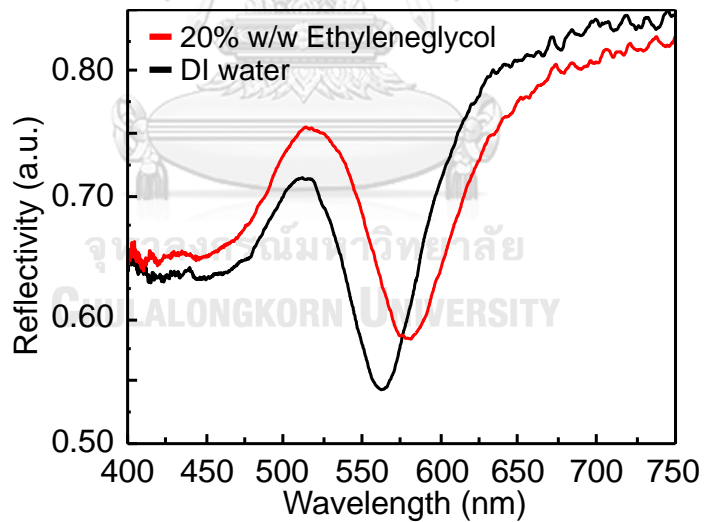
Figure 4.16 SPR reflectivity curves of DI water (n = 1.33) and the solution of 20% w/w Ethylene glycol (n = 1.35). The incident angle was fixed at 63°

As discussed in the above section, the developed miniature SPR sensor chips can be utilized as the sensor that sensitive to the change of refractive index of the dielectric media. We further utilized the SPR to monitor the surface modification through the change of the SPR dip. As shown in Figure 4.17, The SPR dip redshift from 603 to 607 nm after the formation of self-assembly monolayer (SAM) of 1,8 ODT. After modification by AgNPs, the SPR dips further redshift to 620 nm.
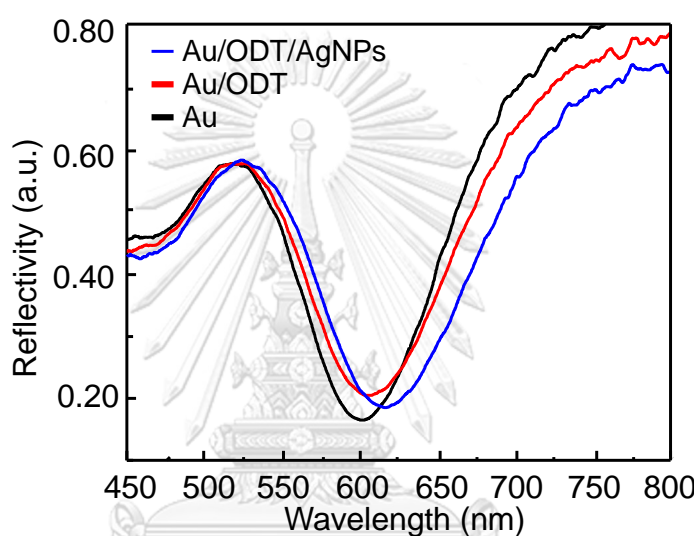
Figure 4.17 SPR reflectivity curves obtained during surface modification as the deposition of silver nanoparticles (AgNPs) on the surface of the SPR sensor chip. 1,8-Octanedithiol (ODT) was utilized as the linker between the gold surface and AgNPs. The incident angle was fixed at 82°

CHAPTER V

CONCLUSIONS

In summary, we have successfully prepared the Sylgard 184 and NOA 61 plano-convex lenses using the confined sessile drop techniques, which take advantage of the sharp edge that resist the spreading of liquids. The developed technique is not only simple and effective but also is capable of large scale production. The hemispherical liquid polymer droplet form on the lens substrates. The lens geometry can be precisely controlled by adjusting the amount of the liquid polymer. The fabricated Sylgard 184 and NOA 61 plano-convex lens provide the magnification up to 51.0X and 88.3X (without a digital zoom), respectively. The plano-convex lens is utilized as an external attachment converting the smartphone camera to become the smartphone microscope. It can observe the small objects such as the makers on the printed circuit board, and default on the bolt. Furthermore, the NOA 61 plano-convex lens can act as the optical prism that utilized in surface plasmon application. The developed miniature NOA 61 SPR sensor chip provides the disposable and economic miniature SPR platform benefiting the utilization of SPR in a small budget

REFERENCES

1. Zhu, X.; Zhu, L.; Chen, H.; Li, Z.; Zhang, W., Fabrication of high numerical aperture micro-lens array based on drop-on-demand generating of water-based molds. *Optics and Laser Technology* **2015,** *68*, 23-27.

2. Tang, C. Y.; Zhang, X.; Chai, Y.; Hui, L.; Tao, L.; Tsang, Y. H., Controllable parabolic lensed liquid-core optical fiber by using electrostatic force. *Optics Express* **2014,** *22* (17), 20948-20953.

3. Li, X.; Li, X.; Shao, J.; Tian, H.; Jiang, C.; Luo, Y.; Wang, L.; Ding, Y., Shape-controllable plano-convex lenses with enhanced transmittance via electrowetting on a nanotextured dielectric. *Journal of Materials Chemistry C* **2016,** *4* (39), 9162-9166.

4. D. Hoheisel, e. a., Fabrication of adhesive lenses using free surface shaping. *Journal of the european optical society-rapid publications* **2013**, *8*, 13065.

5. Lee, W. M.; Upadhya, A.; Reece, P. J.; Phan, T. G., Fabricating low cost and high performance elastomer lenses using hanging droplets. *Biomedical Optics Express* **2014,** *5* (5), 1626-1635.

6. Fuh, Y.-K.; Lai, Z.-H., A fast processing route of aspheric polydimethylsiloxane lenses array (APLA) and optical characterization for smartphone microscopy. *Optics Communications* **2017,** *385*, 160-166.

7. McDonald, C.; McGloin, D., Low-cost optical manipulation using hanging droplets of SYLGARD 184. *RSC Adv.* **2015,** *5* (68), 55561-55565.

8. Fuh, Y. K.; Chen, P. W.; Lai, Z. H., Mechanically tunable aspheric lenses via additive manufacture of hanging elastomeric droplets for microscopic

applications. *Journal of Modern Optics* **2016,** *63* (12), 1129-1135.

9.   Shih, T.-K.; Chen, C.-F.; Ho, J.-R.; Chuang, F.-T., Fabrication of SYLGARD 184 (polydimethylsiloxane) microlens and diffuser using replica molding. *Microelectronic Engineering* **2006,** *83* (11-12), 2499-2503.

10. Ren, H.; Xu, S.; Liu, Y.; Wu, S.-T., A plano-convex/biconvex microlens array based on self-assembled photocurable polymer droplets. *Journal of Materials Chemistry C* **2013,** *1* (44), 7453-7458.

11. Eom, S.-H.; Wrzesniewski, E.; Xue, J., Close-packed hemispherical microlens arrays for light extraction enhancement in organic light-emitting devices. *Organic Electronics* **2011,** *12* (3), 472-476.

12. Ho, Y. H.; Chen, K. Y.; Peng, K. Y.; Tsai, M. C.; Tian, W. C.; Wei, P. K., Enhanced light out-coupling of organic light-emitting diode using metallic nanomesh electrodes and microlens array. *Optics Express* **2013,** *21* (7), 8535-8543.

13. Chen, M.; Gu, G.; Zhang, B.; Cai, Z.; Wei, L., Self-assembled on-chip spherical-cap-shaped microresonators for high sensitivity temperature sensing. *Optics Express* **2016,** *24* (23), 26948-26955.

14. Hu, J.-Y.; Lin, C.-P.; Hung, S.-Y.; Yang, H.; Chao, C.-K., Semi-ellipsoid microlens simulation and fabrication for enhancing optical fiber coupling efficiency. *Sensors and Actuators A: Physical* **2008,** *147* (1), 93-98.

15. Liu, H.; Reilly, S.; Herrnsdorf, J.; Xie, E.; Savitski, V. G.; Kemp, A. J.; Gu, E.; Dawson, M. D., Large radius of curvature micro-lenses on single crystal diamond for application in monolithic diamond Raman lasers. *Diamond and*

Related Materials **2016,** *65*, 37-41.

16.   Sung, Y. L.; Jeang, J.; Lee, C. H.; Shih, W. C., Fabricating Optical Lenses by Inkjet Printing and Heat-Assisted *In Situ* Curing of Polydimethylsiloxane for Smartphone Microscopy. *Journal of Biomedical Optics* **2015,** *20* (4), 047005.

17.   Ekgasit, S.; Kaewmanee, N.; Jangtawee, P.; Thammacharoen, C.; Donphoongpri, M., Elastomeric SYLGARD 184 Planoconvex Lenses Fabricated by a Confined Sessile Drop Technique. *ACS Applied Materials & Interfaces* **2016,** *8* (31), 20474-20482.

18.   Roy, E.; Voisin, B.; Gravel, J. F.; Peytavi, R.; Boudreau, D.; Veres, T., Microlens array fabrication by enhanced thermal reflow process: Towards efficient collection of fluorescence light from microarrays. *Microelectronic Engineering* **2009,** *86* (11), 2255-2261.

19.   Luo, Y.; Wang, L.; Ding, Y.; Wei, H.; Hao, X.; Wang, D.; Dai, Y.; Shi, J., Direct fabrication of microlens arrays with high numerical aperture by ink-jetting on nanotextured surface. *Applied Surface Science* **2013,** *279*, 36-40.

20.   Damodara, S.; George, D.; Sen, A. K., Single step fabrication and characterization of SYLGARD 184 micro lens and its use in optocapillary flow manipulation. *Sensors and Actuators B: Chemical* **2016,** *227*, 383-392.

21.   Amarit, R.; Kopwitthaya, A.; Pongsoon, P.; Jarujareet, U.; Chaitavon, K.; Porntheeraphat, S.; Sumriddetchkajorn, S.; Koanantakool, T., High-Quality Large-Magnification Polymer Lens from Needle Moving Technique and Thermal Assisted Moldless Fabrication Process. *PLoS One* **2016,** *11*, e0146414.

22.   Karunakaran, B.; Tharion, J.; Dhawangale, A. R.; Paul, D.; Mukherji, S.,

Fabrication of miniature elastomer lenses with programmable liquid mold for smartphone microscopy: curing polydimethylsiloxane with in situ curvature control. *Journal of Biomedical Optics* **2018,** *23* (2), 1-14.

23.   Xuefeng, Z.; Hongrui, J., Polydimethylsiloxane Microlens Arrays Fabricated Through Liquid-Phase Photopolymerization and Molding. *Journal of Microelectromechanical Systems* **2008,** *17* (5), 1210-1217.

24.   Surdo, S.; Diaspro, A.; Duocastella, M., Microlens fabrication by replica molding of frozen laser-printed droplets. *Applied Surface Science* **2017,** *418*, 554-558.

25.   Kim, Y. K.; Ju, J. H.; Kim, S. M., Replication of a glass microlens array using a vitreous carbon mold. *Optics Express* **2018,** *26* (12), 14936-14944.

26.   Cruz-Campa, J. L.; Okandan, M.; Busse, M. L.; Nielson, G. N., Microlens rapid prototyping technique with capability for wide variation in lens diameter and focal length. *Microelectronic Engineering* **2010,** *87* (11), 2376-2381.

27.   Di, S.; Chen, X.-y.; Du, R.-x.; Wang, Y.-l.; Zhou, Z.-p.; Wang, Q.-k., The controlling of microlens contour by adjusting developing time in the thermal reflow method. In *International Symposium on Photoelectronic Detection and Imaging 2009: Material and Device Technology for Sensors*, 2009.

28.   Hsieh, H. T.; Lin, V.; Hsieh, J. L.; Su, G. D. J., Design and Fabrication of Long Focal Length Microlens Arrays. *Optics Communications.* **2011,** *284* (21), 5225.

29.   Wang, M.; Yu, W.; Wang, T.; Han, X.; Gu, E.; Li, X., A novel thermal reflow method for the fabrication of microlenses with an ultrahigh focal number. *RSC Advances* **2015,** *5* (44), 35311-35316.

30. Zhou, Z.; Ren, H., Polymeric microlens array formed directly on glass plate. *Optical Engineering* **2017,** *56* (1), 015106.

31. Xia, J.; Qu, D.; Yang, H.; Chen, J.; Zhu, W., Self assembly polymer microlens array for integral imaging. *Displays* **2010,** *31* (4-5), 186-190.

32. Xu, Q.; Dai, B.; Huang, Y.; Wang, H.; Yang, Z.; Wang, K.; Zhuang, S.; Zhang, D., Fabrication of polymer microlens array with controllable focal length by modifying surface wettability. *Opt Express* **2018,** *26* (4), 4172-4182.

33. Blattmann, M.; Ocker, M.; Zappe, H.; Seifert, A., Jet printing of convex and concave polymer micro-lenses. *Optics Express* **2015,** *23* (19), 24525-24536.

34. Wang, L.; Luo, Y.; Liu, Z.; Feng, X.; Lu, B., Fabrication of microlens array with controllable high NA and tailored optical characteristics using confined ink-jetting. *Applied Surface Science* **2018,** *442*, 417-422.

35. Nootchanat, S.; Jaikeandee, W.; Yaiwong, P.; Lertvachirapaiboon, C.; Shinbo, K.; Kato, K.; Ekgasit, S.; Baba, A., Fabrication of Miniature Surface Plasmon Resonance Sensor Chips by Using Confined Sessile Drop Technique. *ACS Applied Material & Interfaces* **2019,** *11* (12), 11954-11960.

36. Seethapathy, S.; Gorecki, T., Applications of polydimethylsiloxane in analytical chemistry: a review. *Analytica Chimica Acta* **2012,** *750*, 48-62.

37. Kim, J. J.; Lee, Y.; Kim, H. G.; Choi, K. J.; Kweon, H. S.; Park, S.; Jeong, K. H., Biologically inspired LED lens from cuticular nanostructures of firefly lantern. *Proceeding of the National Academy of Sciences iof the United States of Americ̈a* **2012,** *109* (46), 18674-18678.

38. Olivieri, F.; Todino, M.; Coppola, S.; Vespini, V.; Pagliarulo, V.; Grilli, S.;

Ferraro, P., Fabrication of polymer lenses and microlens array for lab-on-a-chip devices. *Optical Engineering* **2016,** *55* (8), 081319.

39. Lisensky, G. C.; Campbell, D. J.; Beckman, K. J.; Calderon, C. E.; Doolan, P. W.; Ottosen, R. M.; Ellis, A. B., Replication and Compression of Surface Structures with Polydimethylsiloxane Elastomer. *Journal of Chemical Education* **1999,** *76* (4), 537-541.

40. Cai, L. H.; Kodger, T. E.; Guerra, R. E.; Pegoraro, A. F.; Rubinstein, M.; Weitz, D. A., Soft Poly(dimethylsiloxane) Elastomers from Architecture-Driven Entanglement Free Design. *Adv Mater* **2015,** *27* (35), 5132-5140.

41. Wong, E. J., Modeling and Control of Rapid Cure in Polydimethylsiloxane (SYLGARD 184) for Microfluidic Device Applications. PhD Thesis, Massachusetts Institute of Technology, 2010.

42. Dow Corning® 184 Silicone Elastomer; MSDS No. 11-1252C-01 [Online]; The Dow Corning Corporation, Midland, Michigan, USA, Retrieved September 3, 2017 from https://ostec-materials.ru/upload/iblock/7a8/7a883 bdf5b97631e2b73286987ffdc96.PDF

43. SYLGARD^{TM} 184 Silicone Elastomer; MSDS No. 11-3184101 C [Online]; The Dow Chemical Company, California, USA, Retrieved September 3, 2017 from https://www.dow.com/en-us/pdp.Sylgard-184-silicone-elastomer-kit.010 64291z.html

44. Mark, J. E., Some interesting things about polysiloxanes. *Accounts of Chemical Research* **2004,** 37 (12), 946-953.

45. Wolf, M. P.; Salieb-Beugelaar, G. B.; Hunziker, P., PDMS with designer

functionalities—Properties, modifications strategies, and applications. *Progress in Polymer Science* **2018,** *83*, 97-134.

46.   Harding, D. R.; Goodrich, H.; Caveglia, A.; Anthamatten, M., Effect of temperature and volume on the tensile and adhesive properties of photocurable resins. *Journal of Polymer Science Part B: Polymer Physics* **2014,** *52* (14), 936-945.

47.   Castriota, M.; Fasanella, A.; Cazzanelli, E.; De Sio, L.; Caputo, R.; Umeton, C., In situ polarized micro-Raman investigation of periodic structures realized in liquid-crystalline composite materials. *Opt Express* **2011,** *19* (11), 10494-10500.

48.   Carlborg, C. F.; Haraldsson, T.; Oberg, K.; Malkoch, M.; van der Wijngaart, W., Beyond PDMS: off-stoichiometry thiol-ene (OSTE) based soft lithography for rapid prototyping of microfluidic devices. *Lab Chip* **2011,** *11* (18), 3136-47.

49.   Machado, T. O.; Sayer, C.; Araujo, P. H. H., Thiol-ene polymerisation: A promising technique to obtain novel biomaterials. *European Polymer Journal* **2017,** *86*, 200-215.

50.   Zhou, Z.; Wada, K.; Zhang, M.; Deng, Q.; Shi, L.; Pang, H.; Cao, A.; Hu, S., Fabrication of nano-pillar with sub-100nm resolution based on thiol-ene. In *Nanophotonics and Micro/Nano Optics II*, **2014**, *9277*, 92771U.

51.   Norland Optical Adhesive 61 (NOA61); SDS [Online]; Norland Products Inc , Cranbury, NJ 08512 USA, Retrieved September 3, 2019 from https://www.norlandprod.com/adhesives/NOA%2061.html

52.   Han, M.-W.; Rodrigue, H.; Cho, S.; Song, S.-H.; Wang, W.; Chu, W.-S.; Ahn, S.-H., Woven type smart soft composite for soft morphing car spoiler.

Composites Part B: Engineering **2016,** *86*, 285-298.

53. Nussbaum, P.; Völkel, R.; Roulet, J. C.; Verpoorte, S.; Weible, K. J.; Bruno, A. E.; Herzig, H. P., Design, fabrication and testing of microlens arrays for sensors and microsystems. *Journal of Optics A: Pure and Applied Optics* **1997**, *6* (6), 617-636.

54. Berthier, E.; Beebe, D. J., Flow rate analysis of a surface tension driven passive micropump. *Lab Chip* **2007,** *7* (11), 1475-1478.

55. Zhou, J.; Qi, Q.; Wang, C.; Qian, Y.; Liu, G.; Wang, Y.; Fu, L., Surface plasmon resonance (SPR) biosensors for food allergen detection in food matrices. *Biosens Bioelectron* **2019,** *142*, 111449.

56. Zhao, S. S.; Bukar, N.; Toulouse, J. L.; Pelechacz, D.; Robitaille, R.; Pelletier, J. N.; Masson, J. F., Miniature multi-channel SPR instrument for methotrexate monitoring in clinical samples. *Biosens Bioelectron* **2015,** *64*, 664-70.

57. Fathi, F.; Rahbarghazi, R.; Rashidi, M. R., Label-free biosensors in the field of stem cell biology. *Biosens Bioelectron* **2018,** *101*, 188-198.

58. Michaelis, S.; Wegener, J.; Robelek, R., Label-free monitoring of cell-based assays: combining impedance analysis with SPR for multiparametric cell profiling. *Biosens Bioelectron* **2013,** *49*, 63-70.

59. Nelson, S.G., Johnston, K.S., Yee, S.S., High sensitivity surface plasmon resonace sensor based on phase detection. *Sensors and Actuators B: Chemical* **1996**, *35* (1–3), 187–191.

60. Gupta, B. D.; Verma, R. K., Surface Plasmon Resonance-Based Fiber Optic

Sensors: Principle, Probe Designs, and Some Applications. *Journal of Sensors* **2009,** *2009*, 1-12.

61.   Leong, H.-S.; Guo, J.; Lindquist, R. G.; Liu, Q. H., Surface plasmon resonance in nanostructured metal films under the Kretschmann configuration. *Journal of Applied Physics* **2009,** *106* (12).

62.   Nguyen, H. H.; Park, J.; Kang, S.; Kim, M., Surface plasmon resonance: a versatile technique for biosensor applications. *Sensors (Basel)* **2015,** *15* (5), 10481-10510.

63.   Michael B.J. Exploration of grating-based surface plasmon resonance systems for wave vector matching to enhance plasmon modes and preliminary surface plasmon-enhanced fluorescence interrogation. Master Thesis, Iowa State University, Ames, Iowa, 2016.

64.   Wahid, M. H. A.; Murat, N. F.; Mukhtar, W. M.; Menon, P. S.; Abdul Rashid, A. R.;   Ahmad Dasuki, K.; Awangku Yussuf, A. A. R., Influence of electromagnetic (EM) waves polarization modes on surface plasmon resonance. *EPJ Web of Conferences* **2017,** *162,* 1008.

65.   Oliver, j. F.; Huh, C.; Mason, S. G. Resistance to Spreading of Liquids by Sharp Edges. *Journal of Colloid and Interface Science* **1977**, *59* (3), 568−581.

66.   Fang, G.; Amirfazli, A., Understanding the edge effect in wetting: a thermodynamic approach. *Langmuir* **2012,** *28* (25), 9421-30.

67.   Dimitrakopoulos, P., Gravitational effects on the deformation of a droplet adhering to a horizontal solid surface in shear flow. *Physics of Fluids* **2007,** *19* (12).

68.   Lubarda, V. A.; Talke, K. A., Analysis of the equilibrium droplet shape based on an ellipsoidal droplet model. *Langmuir* **2011,** *27* (17), 10705-10713.

69.   Zhang, H.; Zhao, Y.; Lv, R.; Yang, C., Freezing of sessile water droplet for various contact angles. *International Journal of Thermal Sciences* **2016,** *101*, 59-67.

70.   1951 USAF Targets; Database [Online]; Thorlabs Inc. Newton, New Jersey, USA, Retrieved January 23, 2018 from https://www.thorlabs.com/newgroup page9.cfm?objectgroup_id=4338&gclid=Cj0KCQjwrrXtBRCKARIsAMbU6bF KYsOkGySCU8RfbrQ9I8SASTrMmF9OgOqZBWjHZSlDHrhF97iKoBkaAu6u EALw_wcB.

71.   Lasch, P.; Naumann, D., Spatial resolution in infrared microspectroscopic imaging of tissues. *Biochimica et Biophysica Acta (BBA) - Biomembranes* **2006,** *1758* (7), 814-829.

72.   Edmund Optics Ltd. UK. Pixel Sizes and Optics. Retrieved April 5, 2019, from https://www.edmundoptics.eu/resources/application-notes/imaging/pixel-sizes-and-optics/

73.   Latychevskaia, T., Lateral and axial resolution criteria in incoherent and coherent optics and holography, near- and far-field regimes. *Applied Optics* **2019,** *58* (13), 3597-3603.

74.   I. Prudyus, V. Tkachenko, P. Kondratov, S. Fabirovskyy, L. Lazko, A. Hryvachevskyi., Factors affecting the quality of formation and resolution of images in remote sensing systems, *Computational Problems of Electrical Engineering: Lviv Politechnic National University*, **2015**, *5* (1), 41-46.

75.   Simon H.; Julian Ch. Apple iPhone 7 vs. iPhone 7 Plus: Smartphone specs comparison. Retrieved April 15, 2019, from https://www.digitaltrends. com/mobile/iphone-7-vs-iphone-7-plus/

76.   Übergizmo. What is PPI: Pixels per inch, display resolution. Retrieved April 15, 2019, from http://www.ubergizmo.com/what-is/ppi-pixels-per-inch/

77.   Kihm, K. D., Surface plasmon resonance reflectance imaging technique for near-field (~100 nm) fluidic characterization. *Experiments in Fluids* **2009,** *48* (4), 547-564.

78.   Kihm, K. D.; Cheon, S.; Park, J. S.; Kim, H. J.; Lee, J. S.; Kim, I. T.; Yi, H. J., Surface plasmon resonance (SPR) reflectance imaging: Far-field recognition of near-field phenomena. *Optics and Lasers in Engineering* **2012,** *50* (1), 64-73.

79.   Kushwaha, A. S.; Kumar, A.; Kumar, R.; Srivastava, S. K., A study of surface plasmon resonance (SPR) based biosensor with improved sensitivity. *Photonics and Nanostructures - Fundamentals and Applications* **2018,** *31*, 99-106.

80.   Brahmachari, K.; Ray, M., Effect of prism material on design of surface plasmon resonance sensor by admittance loci method. *Frontiers of Optoelectronics* **2013,** *6* (2), 185-193.

81.   Fogg, E. T.; Hixson, A. N.; Thompson, A. R. Densities and Refractive Indexes for Ethylene Glycol-Water Solutions. *Analytical Chemistry* **1955**, *27*, 1609−1611.

VITA

NAME	Wisansaya Jaikeandee
DATE OF BIRTH	17 Febuary 1994
PLACE OF BIRTH	Saraburi
INSTITUTIONS ATTENDED	Department of Chemistry, Faculty of Science, Kasetsart University
HOME ADDRESS	7 Moo.4 Phaotalardkeaw, Thawung, Lopburi, Thailand

PUBLICATION Nootchanat, S.; Jaikeandee, W.; Yaiwong, P.; Lertvachirapaiboon, C.; Shinbo, K.; Kato, K.; Ekgasit, S.; Baba, A., Fabrication of Miniature Surface Plasmon Resonance Sensor Chips by Using Confined Sessile Drop Technique. ACS Appl Mater Interfaces 2019, 11 (12), 11954-11960.

Jaikeandee, W.; Ekgasit, S.; Nootchanat, S.; Jangtawee, P.; Suriya. P.; Lertvachirapaiboon, C.; Shinbo, K.; Kato, K.; Baba, A, Fabrication of High Magnification Microscope Lens using Confined Sessile Drop Technique. Proceeding of the 8th International Polymer Conference of Thailand, Thailand, 14th-15th , June 2018. pp 165-169.

จุฬาลงกรณ์มหาวิทยาลัย

CHULALONGKORN UNIVERSITY